UCRL-10620

University of California

Ernest O. Lawrence Radiation Laboratory

THE ABSOLUTE INTENSITY OF C_2 SWAN BANDS

TWO-WEEK LOAN COPY

This is a Library Circulating Copy which may be borrowed for two weeks. For a personal retention copy, call Tech. Info. Division, Ext. 5545

DISCLAIMER

This document was prepared as an account of work sponsored by the United States Government. While this document is believed to contain correct information, neither the United States Government nor any agency thereof, nor the Regents of the University of California, nor any of their employees, makes any warranty, express or implied, or assumes any legal responsibility for the accuracy, completeness, or usefulness of any information, apparatus, product, or process disclosed, or represents that its use would not infringe privately owned rights. Reference herein to any specific commercial product, process, or service by its trade name, trademark, manufacturer, or otherwise, does not necessarily constitute or imply its endorsement, recommendation, or favoring by the United States Government or any agency thereof, or the Regents of the University of California. The views and opinions of authors expressed herein do not necessarily state or reflect those of the United States Government or any agency thereof or the Regents of the University of California.

Research and Development

UCRL-10620
UC-4 Chemistry
TID-4500 (19th Ed.)

UNIVERSITY OF CALIFORNIA

Lawrence Radiation Laboratory
Berkeley, California

Contract No. W-7405-eng-48

THE ABSOLUTE INTENSITY OF C_2 SWAN BANDS

Lucy Gay Hagan

(Ph.D. Thesis)

March 18, 1963

Printed in USA. Price $2.50. Available from the
Office of Technical Services
U. S. Department of Commerce
Washington 25, D.C.

THE ABSOLUTE INTENSITY OF C_2 SWAN BANDS

Contents

Abstract v

I. Introduction 1

II. Theory 2

III. Review of Previous Research on the C_2 Swan System

A. Experimental Work 21

B. Theoretical Work 24

IV. Experimental Equipment

A. Furnace Description 40

B. Optical-Pyrometer Calibration 44

C. Concave-Grating Spectrograph 54

D. Photographic Plates 57

E. Instrumentation 58

V. Experimental Procedure 63

VI. Analysis of Data 70

VII. Discussion of Results 79

Acknowledgments 80

Appendix

A. Geometrical Optics Between King Furnace and Concave-Grating Spectrograph 81

B. Tables of Experimental Data 100

References 109

THE ABSOLUTE INTENSITY OF C_2 SWAN BANDS

Lucy Gay Hagan

Inorganic Materials Research Division
and the Department of Chemistry
Lawrence Radiation Laboratory
University of California
Berkeley, California

ABSTRACT

The Swan-band system of the C_2 molecule was produced in emission in a source of thermal equilibrium. The ratio was measured of the intensity in emission and in absorption of certain features of the 0-0 Swan band relative to a blackbody or to a tungsten lamp by using photographic plates and photoelectric scanning techniques. The absolute intensity for the feature was obtained therefore, since the absolute intensity of a blackbody or of a tungsten lamp can be obtained from the Planck equation and the experimentally measured emissivity of tungsten. Experimental results are expressed in terms of the absolute f value or oscillator strength

The absolute f value for the 0-0 Swan band of C_2 in emission is 0.004 ± 0.0007 for the photoelectric scanning experiments on rotational lines, and 0.006 ± 0.004 for emission measurements of rotational lines on photographic plates. For emission experiments at the 0-0 head the f value is 0.007 ± 0.004. Absorption experiments at the 0-0 band head give an f value of 0.005 ± 0.003. The best value for the absolute oscillator strength or f value of the 0-0 band of C_2, obtained by averaging the f values from the emission and absorption data, is 0.005 ± 0.003.

INTRODUCTION

Interest in absolute-intensity measurements arises from the necessity to analyze high-temperature gases to determine concentration of high-temperature molecules, such as C_2 or CN. If an accurate absorption or emission measurement could be made for a gas containing a known amount of C_2 or CN, it would then be possible to determine the amount of C_2 or CN in stars, rocket exhausts, flames, or any high-temperature sources by either an emission or absorption experiment. Lifetime measurements also give emission probabilities and absorption coefficients. The combination of lifetime measurements with absolute-intensity measurements for an equilibrium system will yield equilibrium constants and, through the third law of thermodynamics, enthalpies of formation of high-temperature molecules.

THEORY

The absolute intensity of a high-temperature gas may be measured conveniently in emission. The classically-acceptable measuring technique, however, has been by absorption, because of the difficulty of determining the number of molecules in the excited state. For high-temperature systems in which both the absorbing and emitting states are excited, measurement of absolute intensity by both techniques would prove valuable.

For an absorption experiment the primary datum is the absorption coefficient, k_ν, which is defined by the Beer-Lambert law relation[1]

$$I_\nu = I_\nu^{\,o}\, e^{-k_\nu \ell N''}, \qquad (1)$$

where I_ν and $I_\nu^{\,o}$ are intensities before and after transmission through a column of length ℓ (in cm) of a gas containing N'' absorbing molecules per cm^3. The absorption coefficient, k_ν, varies across an absorption line or band.

The experimental absorption coefficient, k_ν, and the Einstein transition probability for absorption are related. Consider the decrease in intensity of a parallel beam of light, of frequency between ν and $\nu+d\nu$ and of intensity I_ν, traveling in the positive-x direction through a layer of atoms bounded by planes at x and x+dx, of which $\delta N_\nu''$ molecules may absorb in the $\nu+d\nu$ range. The effects of spontaneous re-emission--which takes place in all directions--and of stimulated emission are neglected. The decrease in the intensity of the beam is given by

$$- d[I_\nu \delta\nu] = BI_\nu \delta N_\nu'' dx . \qquad (2)$$

By rewriting Eq. (2), one obtains

$$- \frac{1}{I_\nu} \frac{dI_\nu}{dx} \delta\nu = B\delta N_\nu'' . \qquad (3)$$

The left-hand term is $\delta N_\nu'' k_\nu \delta\nu$, as defined by Eq. (1), and gives

$$\delta N_\nu'' k_\nu \delta\nu = B\delta N_\nu'' . \qquad (4)$$

Integrating over the absorption line then results in a relation between k_ν and B:

$$\int k_\nu d\nu = B, \qquad (5)$$

where B is the probability per second that molecules in the absorbing state will absorb a quantum of light with energy $h\nu$ when exposed to parallel light of intensity I in quanta per sec per cm^2 per frequency interval.

Similarly, the emission coefficient, A, is the probability per second that a molecule in the upper state will spontaneously decay to the lower state with emission of a quantum of light. Einstein has shown that exposure of a molecule to light can also cause induced emission in the same direction as the stimulating light, and that the probability of induced emission is the absorption probability times $\frac{g''}{g'}$, the ratio of degeneracies of the lower and upper states.

Thus the concentration N', in molecules per cm^3, of an excited state of a molecule can be changed by the three processes: spontaneous emission, induced emission, and absorption:

$$- \frac{dN'}{dt} = \frac{1}{4\pi} AN' + B(\frac{g''}{g'})N'I - BN''I. \qquad (6)$$

The intensity of light of wavelength λ emitted by a blackbody of temperature T, in quanta per sec per cm^2 per unit solid angle per unit frequency interval, is given by the Planck equation,

$$I = \frac{2}{\lambda 2} \quad \frac{1}{(e^{\frac{hc}{\lambda kT}} - 1)} , \tag{7}$$

where h is Planck's constant, c is the velocity of light, and k is Boltzman's constant. If light from a blackbody at temperature T is sent from all directions through the gas at temperature T, equilibrium conditions correspond to

$$\frac{dN'}{dt} = 0 = \frac{1}{4\pi} AN' + B(\frac{g''}{g'})N'I - BN''I. \tag{8}$$

By using the Boltzman equation,

$$\frac{N'}{N''} = (\frac{g'}{g''}) e^{-\frac{hc}{\lambda kT}} , \tag{9}$$

where hc/λ corresponds to the energy difference between the two states, one finds

$$I = \frac{A}{4\pi B} (\frac{g'}{g''}) \quad \frac{1}{e^{\frac{hc}{\lambda kT}} - 1} . \tag{10}$$

Comparison of Eqs. (7) and (10) yields the following relationship between the A and B coefficients:

$$\frac{A}{B} = \frac{8\pi}{\lambda^2} \frac{g''}{g'} \tag{11}$$

From Eq. (5), one may then relate absorption results to the emission probability by

$$\int k_\nu d\nu = A(\frac{g'}{g''}) \frac{\lambda^2}{8\pi} . \tag{12}$$

When no other processes depopulate the upper state, the reciprocal of A gives the lifetime of the upper state in seconds.

For small $\ell N''$ the light absorbed by the transition $\ell \rightarrow u$ is

$$I^{\ell u} = \int (I_\nu^{\,o} - I_\nu) d\nu = I_\nu^{\,o} N''\ell \int k_\nu d\nu = I_\nu^{\,o} N''\ell B. \quad (13)$$

The absorption in quanta per sec per cm^2 may also be expressed in terms of the oscillator strength or f value that is related to the electronic transition moment $R^{\ell u}$ and hence to the transition probability for absorption B.

The quantum-mechanical relation between the f value and B for a given frequency[2] is

$$f = \frac{8\pi^2 mc |R^{\ell u}|^2}{3he^2\lambda} = \frac{mcB}{\pi e^2}, \quad (14)$$

where m is the mass and e is the charge of an electron. The transition probability B in intensity units of parallel light used in these equations is related to the original Einstein B coefficients defined in radiation density.*

---

* All equations in this paper are in terms of intensity of light per unit solid angle. The absorption coefficient B for unidirectional light in units of quanta per cm^2 per sec per unit solid angle is related to B for isotropic intensity in units of quanta per cm^2 per sec in all directions, and to B for radiation density in units of quanta per cm^3:

$$B \text{ (unidirectional light)} = \frac{B}{4\pi} \text{ (intensity)} = \frac{B}{c} \text{ (density)}. \quad (15)$$

The Planck equations for unidirectional light for isotropic intensity and for radiation density (in the units defined above and per unit frequency interval) are

$$I\ (\text{unidirectional}) = \frac{2}{\lambda^2} \frac{1}{e^{\frac{hc}{\lambda kT}} - 1}, \tag{7}$$

$$I\ (\text{intensity}) = \frac{8\pi}{\lambda^2} \frac{1}{e^{\frac{hc}{\lambda kT}} - 1}, \tag{16}$$

and

$$I\ (\text{density}) = \frac{8\pi}{c\lambda^2} \frac{1}{e^{\frac{hc}{\lambda kT}} - 1}. \tag{17}$$

The relation for the absolute intensity of emission per unit solid angle for small N', the number of molecules per cm^3 in the upper state, is

$$I^{u\ell} = N'\ell A \frac{1}{4\pi}. \tag{18}$$

The absolute intensity for absorption (abs) or emission (em), both in units of quanta per sec per cm^2 per unit frequency interval per unit solid angle, may be expressed in terms of the f value:

$$I^{\ell u}_{abs} = \frac{\pi e^2 N'' \ell f I_\nu^{\ o}}{mc}, \tag{19}$$

$$I^{u\ell}_{em} = \frac{2\pi e^2 N' \ell f}{mc\lambda^2} \frac{g''}{g'}. \tag{20}$$

The f value on the basis of classical electron theory of dispersion[3] is equal to the ratio, $\frac{M'}{M}$, which was found to be a constant for a particular spectral line. The optical behavior of M atoms per cm^3 was represented by the behavior of M quasi-elastically bound electrons or dispersion electrons. The f value of a spectral

line is a measure of the degree to which the ability of the atom to absorb and emit this line resembles that of a classical oscillating electron. The oscillator strength is related to the electronic transition moment as shown in Eq. (14). The transition moment[4] is equal to

$$R^{u\ell} = \int \psi_u^* \left(\sum_i e \vec{r}_i \right) \psi_\ell \, d\tau \, . \tag{21}$$

The wave functions correspond to the nucleii fixed in their equilibrium configuration for the initial state ψ_ℓ. The vector $\vec{r}_i$ is the radius vector of the ith electron referred to a system of coordinate axes fixed in the molecule. The transition moment vector is obtained by computing $R_x^{u\ell}$, $R_y^{u\ell}$, and $R_z^{u\ell}$, and by adding vectorially. If the molecule has one or more axes of symmetry and if the coordinate axes are taken along and perpendicular to such axes, all but one of the integrals R_x, R_y, R_z vanish. For a given pair of wave functions ψ_u, ψ_ℓ, the $R^{u\ell}$ vector is directed along one of the coordinate axes. Mulliken and Rieke[5] define the dipole strength D as

$$D = \frac{|R^{u\ell}|^2}{e^2} \tag{22}$$

in the notation of this paper. The value of $|R^{u\ell}|^2$ is called the line strength.[6] In theoretical computations it is convenient to tabulate one of the three quantities: line strength, dipole strength or f value.

According to classical theory of radiation,[7,8] the oscillator strengths should obey a sum rule which was proved in the quantum-mechanical theory by Thomas, Reiche, and Kuhn,[9, 10, 11]

$$\sum_{u} f_{u\ell} = \kappa , \tag{23}$$

where u and ℓ denote all quantum numbers and κ is the number of electrons in the system. Bethe and Saltpeter[8] point out that for an ion κ is not equal to the nuclear charge. Mulliken and Rieke[5] made the simplification which is used generally in theoretical calculations of f values: that all those electrons of the electron configuration which remain in unbroken closed shells during the transition may be ignored, and only as many electrons as are present in shells which are broken or formed during transition need be considered. The sum rule then is equal to the number of optically active electrons of the molecule.[12] Mulliken and Rieke further point out the difficulty in theoretical studies of determining the proper combination of wave functions to be used in the linear combination of atomic orbitals (LCAO) for molecules such as C_2. The amount of s,p mixing often has a large influence on the value of $R^{u\ell}$ and is not easy to determine. To find the f value experimentally, the intensity of a band must be known. A method for finding the absolute intensity of a fraction of a band experimentally and relating it to the total-band intensity has been discussed by Robinson and Nicholls, and is used here.[13]

For a band, N' is the number of molecules per cm^3 in the upper state which emit and contribute radiation to the band, and is defined as

$$N' = N'_o \sum_{i} g_i \, e^{-\epsilon_i/kT} = N'_o \, Q^u_{rot} . \tag{24}$$

where N'_o is the number of molecules per cm^3 in the lowest vibrational level of the upper electronic state, and

$$Q^u = Q^u_{e\ell}\, Q^u_{vib}\, Q^u_{rot} \; . \tag{25}$$

For a fraction of a band, N^*_u is the number of molecules per cm^3 contributing radiation to the fraction of the band being measured, and the rotational part of Q is different because the sum is being taken over only a fraction of the rotation lines of the band:

$$N^*_u = N'_o \quad Q^u_{e\ell}\, Q^u_{vib} \sum_{J'=a}^{J'=b} (2J'+1)e^{-\frac{hcB'}{kT}} \quad . \tag{26}$$

The Einstein transition probability of emission for a band[14] is

$$A = \frac{16\pi^3 \nu^3_{u\ell} g''}{3hc^3 g'} \; | R^{u\ell}_e |^2 |R^{\nu'\nu''}_{vib}|^2 \quad . \tag{27}$$

For $\Delta\Lambda = 0$ transitions here considered, $\frac{g''}{g'}$ is equal to unity. Here, R_e is the electronic transition moment and

$$R^{\nu'\nu''}_{vib} = \int \psi'_\nu \, \psi''_\nu \, dr \tag{28}$$

is the overlap integral,[15] the square of which is the Franck-Condon factor. The electronic eigenfunctions depend slightly on the internuclear distance as a parameter, and therefore R_e depends somewhat on r. The Franck-Condon principle as formulated in quantum mechanics is based on the assumption that the variation of R_e with r is slow, and that R_e may be replaced by an average value $\bar{R}_e$. Then for a band the total transition moment is

$$R^{\nu'\nu''} = \bar{R}_e \int \psi'_\nu \, \psi''_\nu \quad dr. \tag{29}$$

For the rotational moment[16,17] for a band, it can be shown that

$$\sum_{J''} \sum_{M'M''} |R_{rot}^{J'J''}|^2 = (2J' + 1), \tag{30}$$

where the summation is over all values of the magnetic quantum numbers M', M'' for a given level ν', J'. Dependence of rotation on vibration would necessitate multiplication of $(2J' + 1)$ by a constant for a given level. For one rotational line of a band, the removal of J dependence from the rotational eignefunctions gives

$$|R_{rot}^{J'J''}|^2 = S_{J'} , \tag{31}$$

where $S_{J'}$ is the strength factor for the rotational line.

For a fraction of a band, by considering the rotational degeneracy, the transition probability is

$$A = \frac{16\pi^3 \sum_{J'=a}^{J'=b} \nu_{u\ell}^3 |R_e^{u\ell}|^2 |R_{vib}^{\nu'\nu''}|^2}{3hc^3 \sum_{J'=a}^{J'=b} (2J' + 1)} \tag{32}$$

For a band, ν can be taken as the average ν for all rotational lines from P, Q, and R branches. A simplifying assumption will be made: for a band ν will be ν_o-- the zero line for the band; for a fraction of a band, ν will be the frequency of each rotational line.

The intensity of the entire band with the use of the more explicit form is

$$I_{\substack{em \\ band}}^{u\ell} = \frac{16\pi^3}{3hc^3} \nu_o^3 N'_o Q_e^u Q_{vib}^u Q_{rot}^u |R_e^{u\ell}|^2 |R_{vib}^{\nu'\nu''}|^2 \tag{33}$$

The intensity for a fraction of a band, by making the proper substitutions, is

$$I^{u\ell}_{em(J'=a \text{ to } J'=b)} = \frac{16\pi^3}{3hc^3} N'_o Q^u_e Q^u_{vib} |R^{u\ell}_e|^2 |R^{v'v''}_{vib}|^2$$

$$\cdot \sum_{J'=a}^{J'=b} S_{J'} \nu^3_{J'J''} e^{-\frac{F'}{kT}} \qquad (34)$$

where F' is the energy emitted in the rotational transition, $J' \rightarrow J''$.

In experimental measurements usually the experimental quantity is the ratio, $\frac{I^{u\ell}(J'=a \text{ to } J'=b)}{I_{BB}}$, where the intensity of the fraction of the band is compared to the intensity of a blackbody in the same wavelength region. Since the absolute intensity of a blackbody can be calculated, the absolute intensity of the band fraction is found. To convert this measured quantity to the theoretically important $I^{u\ell}$, the ratio of the two intensities is taken:

$$\frac{I^{u\ell}_{(J'=a \text{ to } J'=b)}}{I^{u\ell}_{band}} = \frac{\sum_{J'=a}^{J'=b} S_{J'} \nu^3_{J'J''} e^{-\frac{F'}{kT}}}{\nu^3_o Q^u_{rot}} . \qquad (35)$$

The ratio $\frac{\nu^3_{J'J''}}{\nu^3_o}$ is near unity and causes a maximum difference in ratio of three percent for the 0-0 band of the C_2 Swan system. It could be ignored but will be taken into account in the present calculations.

The intensity of emission for a band is then

$$I^{u\ell}_{band} = \frac{I^{u\ell} \nu^3_o Q^u_{rot}}{\sum_{J'=a}^{J'=b} S_{J'} \nu^3_{J'J''} e^{-\frac{F'}{kT}}} = \frac{2\pi e^2 N' \ell f}{mc\lambda^2} \frac{g''}{g'} \qquad (36)$$

from Eq. (20). The f-value may be calculated now from the measured data and Eq. (24), $N' = N'_o Q^u_{rot}$:

$$f = \frac{mc\lambda^2}{2\pi e^2 N'_o \ell} \cdot \frac{I^{u\ell}(J' = a \text{ to } J' = b)}{\frac{\lambda_o^3}{c^3} \sum_{J'=a}^{J'=b} S_{J'} \frac{c^3}{\lambda^3} e^{-\frac{F'}{kT}}} . \tag{37}$$

The intensity of absorption of the band is

$$I^{u\ell}_{\substack{abs \\ band}} = \frac{8\pi^3}{3hc^2} I^{u\ell}_o N''_o{}^{\ell} Q^{\ell}_e Q^{\ell}_{vib} Q^{\ell}_{rot} |R^{\ell u}_e|^2 |R^{\nu''\nu'}_{vib}|^2 , \tag{38}$$

and for a fraction of a band

$$I^{\ell u}_{abs} = \frac{8\pi^3}{3hc^2} I^{\ell u}_o N''_o{}^{\ell} Q^{\ell}_e Q^{\ell}_{vib} |R^{u\ell}_e|^2 |R^{\nu''\nu'}_{vib}|^2$$

$$\cdot \sum_{J''=a}^{J''=b} S_{J''\nu_{J''J'}} e^{-\frac{F''}{kT}} \tag{39}$$

where F'' is the energy absorbed in the rotational transition, $J'' \rightarrow J'$. In absorption, N''_o is the number of molecules absorbing in the lowest vibrational level of the lower electronic state; Q^{ℓ}_e, Q^{ℓ}_{vib}, Q^{ℓ}_{rot}, and $S_{J''}$ refer to the lower electronic state. The ratio of the measured fractional-band intensity referred to the band intensity is then

$$\frac{I^{\ell u}_{(J''=a \text{ to } J''=b)}}{I^{\ell u}_{band}} = \frac{\sum_{J''=a}^{J''=b} S_{J''} e^{-\frac{F''}{kT}}}{Q^{\ell}_{rot}} \tag{40}$$

From this ratio the absolute intensity of the band is found and is substituted into Eq. (19) to obtain the f value. The intensity of absorption for a band may be equated to Eq. (19):

$$I_{band} = \frac{I^{\ell u}_{(J''=a \text{ to } J''=b)}\, Q^{\ell}_{rot}}{\sum_{J''=a}^{J''=b} S_{J''}\, e^{-\frac{F''}{kT}}} = \frac{\pi e^2 N''\, \ell f I^{o}_{\nu}}{mc} \quad . \qquad (41)$$

The f value in terms of absorption data with the use of $N'' = N''_o Q^{\ell}_{rot}$ is

$$f = \frac{mc}{\pi e^2 N''_o\, \ell} \; \frac{I^{\ell u}_{(J''=a \text{ to } J''=b)}}{I^{o}_{\nu} \sum_{J''=a}^{J''=b} S_{J''}\, e^{-\frac{F''}{kT}}} \quad . \qquad (42)$$

The preceding equations describe intensity absorbed or emitted as a linear function of the number of participating atoms. For weak absorptions or emissions these equations will be pertinent; however, for high concentrations of molecules absorbing or emitting, the use of only the first two terms in the expansion of the exponential term

$$e^{-k_{\nu} \ell N} = 1 - k_{\nu} \ell N + \ldots \qquad (43)$$

for absorption is not adequate to describe the phenomenon. Total absorption has been defined[18] as the area of the absorption feature divided by the area of the incident intensity in the same wave number or energy interval. If the interval is expressed in angstrom units the total absorption is the equivalent width. Total absorption is thus

$$A_\lambda = \frac{I_{abs}}{I_o} = \int_{-\infty}^{\infty} \left(1 - e^{-k_\nu \ell N''}\right) d\nu \ , \qquad (44)$$

where I_{abs} is the absorbed energy and I_o the incident energy. Experimentally, a curve of growth is obtained from a log-log plot of the total absorption as a function of number of molecules in the lower state, or A_λ vs $\frac{N'' f\ell}{\text{const } \nu_o} \left(\frac{T}{M}\right)^{1/2}$.

King and King[19,20] discuss the variation of equivalent width with concentration and temperature changes. For small equivalent width and low concentrations the theoretical curve of growth is linear, and the equivalent width A_λ is approximated by

$$A_\lambda = \frac{\pi e^2}{mc^2} \lambda^2 10^{-8} N'' f\ell \ , \qquad (45)$$

whereas for the linear part and lower part of the horizontal portion of the curve, an expansion[21,22] gives

$$\frac{A_\lambda}{2\Delta\lambda_D} = \frac{\sqrt{\pi}}{2} k_o' N'' f\ell \left[1 - \frac{k_o' N'' f\ell}{2!\sqrt{2}} + \frac{(k_o' N'' f\ell)^2}{3!\sqrt{3}} - \frac{(k_o' N'' f\ell)^3}{4!\sqrt{4}} + \ldots\right]. \qquad (46)$$

The expansion term may be represented by a sum, where $C = k_o' N'' f\ell$ for $k_o' N'' f\ell < 3$:

$$\frac{A_\lambda}{2\Delta\lambda_D} = \frac{\sqrt{\pi}}{2} \sum_{n=1}^{\infty} \frac{C^n (-1)^{n+1}}{n!\sqrt{n}} \ . \qquad (47)$$

The expression for k_o' as King and Stockbarger[22] use it is given by

$$k_o' = \frac{e^2 \sqrt{\pi(\ell n2)}}{mc^2} \quad \frac{\lambda}{\Delta\lambda} \quad 10^{-8} \quad , \tag{48}$$

which is the usual absorption coefficient per oscillator, or $k_o N'' \ell f \left(\frac{c}{\lambda}\right)$.

The Doppler breadth in angstrom units is

$$\Delta\lambda_D = \frac{\lambda}{c} \left(2R(\ell n2) \frac{T}{M}\right)^{1/2} . \tag{49}$$

By using Eq. (44) through (46), the equivalent width A_λ may be calculated as a function of $N'' \ell f$. The calculation gives the linear and lower Doppler portions of the curve of growth. The equivalent width must be small to be in this linear region, and therefore a combination of low vapor density and small f value is desired for experimental measurements. King and King[19,20] point out that the main objection to using this portion of the curve is the faintness of the lines and consequent uncertainty in measuring their equivalent widths. The large uncertainty in the measurements of equivalent widths requires many measures on each line. If the factors N'', ℓ, λ, T, and M are known in this region, however, the absolute f value may be derived from observations of the equivalent width. The natural-damping portion of the curve of growth for which A_λ is proportional to $\sqrt{N'' f}$ is sensitive to external influence such as collision broadening; the linear portion and at moderately low pressures the Doppler portion for which A_λ is proportional to $N'' f$ are not influenced by external effects; it is therefore convenient to use the linear part of the curve to measure f values.

In emission for high concentrations of emitters, self-absorption decreases the observed intensity and causes emitted intensity to be a nonlinear function of concentration. An expression for the intensity of emission corrected for self-absorption at a single wavelength may be derived as a function of concentration. Hicks[23] discusses such a derivation. For a column of length ℓ of emitting gas of uniform cross section and temperature, the intensity in quanta per sec per cm^2 emitted by a very thin cross section of the column is $I_\nu^o = N'Ad\ell$, where N' is the number of molecules per cm^3, A is the Einstein coefficient for emission, and $d\ell$ is the element of length. If the cross section is at a distance ℓ down the column, then the intensity of light observed from the cross section may be described by the Beer-Lambert relation

$$I_\nu = I_\nu^o e^{-b_\nu N''\ell} , \tag{50}$$

where b_ν is used for the absorption coefficient to distinguish it from the coefficient for pure absorption k_ν. The absorbed light is then $I_{abs} = I_\nu^o b_\nu N'' d\ell$, a term which is also equal to the rate of absorption $BN''I_{BB}\ell$, where $d\ell$ is the element of length ℓ of a cylinder and I_ν^o is the emission intensity with no self-absorption; I_{BB} is the Planck equation for a blackbody, Eq. (7), in units of quanta per sec per cm^2 area normal to the light per unit solid angle per unit frequency interval. Substituting for I_ν^o in the equation for I_{abs} and subtracting the absorbed energy for I_ν^o, a series expansion is obtained for the measured intensity I_{meas}:

$$I_{meas} = \frac{AN'}{b_\nu N''} \left[b_\nu N'' \ell - \frac{(b_\nu N'' \ell)^2}{2!} + \frac{(b_\nu N'' \ell)^3}{3!} - \ldots \right] \quad (51)$$

$$= \frac{A}{b_\nu} \; e^{-\frac{hc}{\lambda kT}} \left[1 - e^{-b_\nu N'' \ell} \right]. \quad (52)$$

When N' approaches infinity, I_{meas} approaches the intensity of a blackbody I_{BB}, a condition that gives an upper limit to the amount of self-absorption. For the blackbody condition, if self-absorption is great enough to produce complete reversal, then the amount of absorption is equal to the amount of emission, or $I_\nu^o = I_{BB}$, and

$$I_{abs} = I_{em} = I_{BB} b_\nu N'' \ell = N' A \ell; \quad (53)$$

therefore,

$$b_\nu = \frac{A \, e^{-\frac{hc}{\lambda kT}}}{I_{BB}} \quad . \quad (54)$$

Then substituting for b_ν,

$$I_{meas} = I_{BB} \left[1 - e^{-b_\nu N'' \ell} \right] . \quad (55)$$

For intensities altered by self-absorption, a correction factor Q_ν may be obtained by dividing Eq. (53) by Eq. (55). Thus,

$$\frac{I_{em}}{I_{meas}} = Q_\nu = \frac{b_\nu N'' \ell}{1 - e^{-b_\nu N'' \ell}} \quad (56)$$

To find the value of the correction factor Q_ν from experimental data, the ratio of the intensity of the feature to the intensity of a blackbody is required. To obtain the proper ratio, Eq. (55) is written as

$$\frac{I_{meas\ \nu}}{I_{BB}} = R_\nu = 1 - e^{-b_\nu N'' \ell} \quad . \quad (57)$$

Equation (57) expressed in logarithmic form gives

$$b_\nu N''\ell = -\ell n\,(1 - R_\nu)\ , \tag{58}$$

and the correction factor Q_ν is obtained by substitution of Eq. (57) and (58) into Eq. (56):

$$Q_\nu = \frac{-1}{R_\nu}\ \ell n\,(1 - R_\nu)\ . \tag{59}$$

The correction factor Q_ν is useful at a single frequency. To evaluate the correction factor for a Doppler-broadened line, a correction factor for the integrated intensity of the line is required, as Hicks[23] has described. The averaged correction factor Q is obtained by applying Q_ν to the intensity I_ν at each frequency, and integrating over the particular frequency interval of interest:

$$Q = \frac{\int_0^\infty Q_\nu I_\nu d\nu}{\int_0^\infty I_\nu d\nu}\ . \tag{60}$$

The relation[24] between b_ν (the absorption coefficient at a certain frequency) and b_o (the absorption coefficient at the peak of the Doppler line) is

$$b_\nu = b_o\, e^{-\left(2\sqrt{\ell n2}\,\frac{(\nu-\nu_o)}{\Delta\nu_D}\right)^2}\ . \tag{61}$$

Therefore by using the relation for intensity without self-absorption $I_{em} = AN'\ell$ and the reversal condition $b_\nu = \frac{A}{I_{BB}}\ e^{\frac{-hc}{\lambda kT}}$, the expression for I_{em} becomes

$$I_{BB} = N''\ell\ I_{BB}\ b_o\ e^{-\left[2\sqrt{\ell n2}\ \frac{\nu-\nu_o}{\Delta\nu_D}\right]}\ . \tag{62}$$

Equation (59) may be expressed as a series by expanding $\ell n(1-R_\nu)$,

$$Q_\nu = 1 + \frac{R_\nu}{2} + \frac{R_\nu^{\,2}}{3} + \ldots . \tag{63}$$

For small values of R_ν, the second and higher-order terms may be dropped. The expressions for I_{em} and Q_ν are substituted into Eq. (60) and integrated over all frequencies. The blackbody intensity I_{BB} remains constant over the small frequency range of a rotational line. Thus,

$$Q = 1 + \frac{1}{2\sqrt{2}} R_o \quad . \tag{64}$$

The ratio R_o is $\frac{I_{meas}}{I_{BO}}$ if I_{meas} is the area of an observed rotational line with only Doppler broadening and I_{BO} is the area of a triangular feature of blackbody intensity at the peak of the feature and of Doppler width. The Doppler width $\Delta\nu_D$ in frequency units is

$$\Delta\nu_D = \frac{2\sqrt{2R\ell n2}}{\lambda_o} \sqrt{\frac{T}{M}} \ , \tag{65}$$

where R is the gas constant in ergs per mole degree, λ_o is the peak wavelength, T is the temperature and M is the molecular weight of the gas. For a line which is instrumentally broadened more than the Doppler width, the equation[24]

$$\int I_\nu d\nu = \frac{\sqrt{\pi}}{2\sqrt{\ell n2}} I_o \Delta\nu_D \tag{66}$$

relates the area of the broadened feature to the Doppler area. To convert measured areas to Doppler areas, the equation

$$I_o \Delta\nu_D = 0.94 \int I_\nu d\nu \tag{67}$$

is used. This calculated area $I_o \Delta\nu_D$ is used therefore in place of I_{meas} in the ratio R_o, where I_o is the peak intensity of the Doppler feature. When R_o is substituted into Eq. (64), the correction factor Q is obtained. Multiplication of the measured intensity by Q gives intensities corrected for self-absorption.

PREVIOUS RESEARCH ON THE C_2 SWAN SYSTEM

A. Experimental Work

Experimental measurements of the absolute f value have not been reported although preliminary measurements have been made in this laboratory. Intensity measurements in emission relative to the 0-0 band of the Swan system were made in 1932 of five different laboratory sources: Bunsen flame, oxy-coal gas flame, carbon arc in hydrogen, argon discharge tube, and spark under glycerine by Johnson and Tawde.[25] They concluded from vibrational-temperature determinations that there was no statistical equilibrium of excited molecules, and therefore determined the distributions by assuming that the sum of the transition probabilities of all observed bands from each upper vibrational state (v') is a constant. Quantitative light-yield measurements on low-pressure flames for C_2 bands were made by Gaydon and Wolfhard.[26] Previous measurements[27] of rotational temperature had established that excitation in these flames was not of a purely thermal nature, and therefore variations of light yield with mass flow, pressure, and mixture strength were measured. Pressures of C_2, derived from light-yield measurements agree with presently-known equilibrium pressures of C_2. Laud,[28] Patel,[29] and Tawde and Patel[30] have made a series of measurements reported as relative transition probabilities by Tawde and Laud[31] on different types of ethyl-alcohol and oxy-coal flames. Their measured relative transition probabilities are given in Table I.

King[32] made relative intensity measurements in a carbon-resistance-tube furnace and calculated relative transition probabilities. He measured band-head intensities in emission for the C_2 Swan system. From the peak intensity at the head he subtracted the background intensity to get the apparent intensity of the band. King did emission and absorption measurements on the system; the relative transition probabilities by both procedures were in agreement. He reported relative transition probabilities obtained from his emission work. His results are in Table II.

Phillips[33,34] also measured relative intensities of C_2 Swan bands in emission by scanning the spectra with an RCA 1P21 photomultiplier tube, the output of which was fed into a contact-modulated ac amplifier. Initially he measured band profiles by using wide slits so that rotational structures of the bands were not resolved. He found that even with refinements of theory and careful laboratory photometry there were discrepancies in the results. Because the agreement between his and King's laboratory measurements was poor for certain bands, Phillips measured the relative integrated intensities of neighboring rotational lines in the spectral regions where the bands overlapped. To investigate self-absorption he defined an equivalent width of an emission line analogous to that in absorption because the intensity of an emission feature approaches blackbody intensity as the concentration of the emitting gas increases. He then used the theory of the curve of growth to relate equivalent width to number of emitters. The equivalent width was found experimentally to vary from 0.0023 to 0.0028A, depending on the

effective length of the emitting column. By assuming that the profiles of the lines were thermal and by using the curve-of-growth theory, it was found that at 3000°K the self-absorption is negligible for equivalent widths below 0.004. He concluded, therefore, that no corrections need be made for the effect of self-absorption. He found for the 1-1 band closer agreement with King's value, which indicated that the previously-used technique of integrated-band profiles may yield uncertain results for intrinsically weak features. The transition probabilities relative to each leading band were considered to be much more reliable than the transition probabilities relative to the 0-0 band. The determinations, compared with the results of his previous studies, reduced the relative transition probability of the 1-0 band and increased that of the 0-1 band shown in Table II.

B. Theoretical Work

Lyddane, Rogers, and Roach[35] used atomic orbital (AO) and molecular orbital (MO) approximations to find a ratio of f values for CN and C_2. Then the f value of C_2 was obtained from this ratio by using the experimental f value for CN.[36] The absolute f value for the C_2 Swan system was calculated to be 0.024. Stephenson[37] used linear combinations of atomic-wave orbitals (LCAO) to approximate wave functions for the molecular orbitals $(\sigma_u 2s) \rightarrow (\sigma_g 2p)$, where $\sigma 2s$ and $\sigma 2p$ indicate m = 0 in atomic notation, and g,u describe the wave function with respect to its center as symmetrical or antisymmetrical, respectively. He therefore assumes that the inner shells do not participate in the one-electron transfer, 2s → 2p, and calculates an absolute f value and lifetime for the Swan system of 0.029 and 1.4×10^{-7} sec, respectively.

The complete molecular-orbital designation of the $^3\Pi_u$ and $^3\Pi_g$ levels in C_2 is as follows:

$$^3\Pi_u \ (K)(K)\ (z\sigma_g)^2\ (y\sigma_u)^2\ (w\pi_u)^3\ (x\sigma_g)$$

and

$$^3\Pi_g \ (K)(K)\ (z\sigma_g)^2\ (y\sigma_u)\ \ (w\pi_u)^3\ (x\sigma_g)^2 \quad .$$

The molecular-orbital notation of Mulliken[38] and discussed by Coulson[39] is given:

Full notation	Abbreviated notation
$\sigma 1s$	K
$\sigma^* 1s$	K
$\sigma 2s$	$z\sigma$
$\sigma^* 2s$	$y\sigma$
$\sigma 2p$	$x\sigma$
$\pi_y 2p$	
$\pi_z 2p$	$w\pi$

(continued next page)

(continued from page 24.)

Full notation	Abbreviated notation
π_y^*2p	$v\pi$
σ^*2p	$u\sigma$

The σ and σ^* orbitals are bonding and antibonding orbitals filled with two electrons whereas π and π^* refer to bonding and antibonding orbitals filled with four electrons.

The advantage of Mulliken's notation is that it may be made to apply to heteronuclear molecules. The notation $z\sigma$ means that the lowest molecular orbital of the σ type will normally be compounded, but not completely, of 2s atomic orbitals.

Shull[40,41,42] used LCAO's for molecular orbitals, assumed that orbitals not directly involved were unaffected by the transition, and thereby reduced the transition to a one-electron problem, $(y\sigma_u) \rightarrow (x\sigma_g)$. His method of approach is thus analogous to Stephenson's.

Shull[40] first calculated the f value for the Swan transition with the use of the dipole-length method and used the conventional transition-moment integral,

$$Q_z = \int \psi_u \left(\sum_i z_i\right) \psi_\ell \, d\tau \, , \tag{68}$$

where the sum is over the i electrons for the radial z component, and reported for the f value, 0.13. Later Schull[41,42] used the dipole-velocity method and the integral

$$Q_v = \int \psi_u \left(\sum_i \frac{\partial}{\partial z_i}\right) \psi_\ell \, d\tau \, , \tag{69}$$

where the gradient of the radial z component is used in the integral.

His atomic functions which make up the linear combination were either Slater functions or self-consistent field functions fitted by exponentials of Slater form. For the dipole-length calculation he calculated the f value as a function of atomic-orbital form and as a function of hybridization of 2s and σ2p orbitals. The oscillator strengths were found to be insensitive to the forms used for atomic orbitals but relatively sensitive to hybridization in the region of low hybridization.

From the dipole-velocity calculations Shull concluded that the degree of hybridization was higher than his previous estimate of 8 to 17 % hybridization for an f value of 0.13. He found that the value of f dropped when he used orthogonal Slater 2s functions. A change of Z(effective atomic number) had a large effect on the oscillator strength as a function of hybridization. He reports a best-average f value of 0.18 obtained from the respective intersections of the dipole-velocity and dipole-length curves for the limiting pairs $Z_{x\sigma_g} = 3.90, 3.90$; $Z_{y\sigma_u} = 3.25, 2.60$. His calculation indicated the presence of about 25% hybridization

Coulson and Lester's[43] calculation of the square of the transition moment for C_2 included the effect of both hybridization and orthogonalization on the wave functions. They conclude that orthogonalization seems somewhat less important for f-value calculations than for calculations in energy. They used Z = 3.08 and for their simplest calculation used no orthogonalization. In the second approximation they used orthogonal atomic-wave functions; for the third approximation they orthogonalized their molecular orbitals. Finally

they used the best hybrids of s and p and included orthogonalization. Including hybridization increased the oscillator strength by a factor of the order of ten, and they estimate for the oscillator strength for the Swan system 0.24. They point out that Shull who omitted orthogonalization and Stephenson who omitted orthogonalization and hybridization found 0.13 and 0.029, respectively. Coulson and Lester conclude that if configuration interaction is neglected, except when included implicitly in the use of hybrid orbitals, then reasonable oscillator strengths are not obtained unless hybridization and orthogonalization are included.

Oscillator strengths for nine electronic transitions among the low-lying excited states of C_2 have been calculated by Clementi.[44] He used the dipole-moment-operator method and Slater-type functions with Z = 3.25. To calculate the amount of hybridization, he used Mulliken's semi-empirical method[45] for estimating a constant-core energy (the contribution to the total energy due to core electrons and nuclei). To the core energy is added the energy of the valence electrons to give the total energy Clementi found 1.0% hybridization of the $2\sigma_u$ orbital and approximates the other Swan transition orbital, $3\sigma_g$, to be the same.

Clementi reports an f value of 0.0485 for the Swan system, a value comparable to that of Lyddane, Rogers, and Roach (0.024) and of Stephenson (0.029). Shull's calculation for the Swan system of f = 0.13 or 0.18 and Coulson's value of 0.24 are somewhat higher. Only a reliable experimental value can resolve these differences. Table II summarizes these theoretical absolute f values.

Pillow[46,47] has calculated relative transition probabilities for Swan bands. She used three different forms of graphical "distortions" of harmonic-oscillator wave functions to fit a Morse[48] potential, the basic technique proposed by Gaydon and Pearse.[49] Ta-You Wu[50] has pointed out that this method is good only for low vibrational states because for the higher states of an anharminic oscillator the wave functions are no longer orthogonal. He suggested the use of a Morse-potential function and the application of the Wentzel[51] - Kramers[52] - Brillouin[53] (WKB) method of solution of the Schroedinger equation to find vibrational wave functions of an anharmonic oscillator. Solutions are Bessel functions. Wyller[54] applied this technique with the use of the Hulburt-Hirschfelder[55,56] potential, which he considered more accurate than the Morse function, to vibrational bands of the Swan system of C_2, and obtained relative transition probabilities. His wave functions when properly normalized decreased his values of relative transition probabilities from 1 to 10 %. He points out that Pillow's calculations are closer to the experimental values of King, whereas the WKB values are closer to the experimental values of Johnson and Tawde. Table IV lists calculated relative transition probabilities for Pillow and Wyller.

Hutchisson[57] solved the wave equation for the harmonic oscillator and obtained wave functions as Hermite polynomials. Wurm[58] used Hutchisson's integrals as a first approximation to calculate relative transition probabilities for Swan bands. McKellar and Buscombe[59] by using improved molecular constants and Hutchisson's integrals obtained values different from those of Wurm. The difference between

the equilibrium atomic separations for the two electronic states, Δr_e, is an important value for Hutchisson's method as well as for Morse's function. Wyller showed that changes of Δr_e produce less of a deviation with the Hulburt-Hirschfelder method. Tawde and Patel[60] who also used the Hutchisson method found values they reported to be different from those of McKellar and Buscombe. However, on re-checking the calculations in both reports, McKellar and Tawde[61] later state that their differences are not large and are accounted for by the different Δr_e's, 0.046, and 0.047A they used. They point out that the two calculations illustrate the considerable sensitivity of the calculated relative transition probabilities to Δr_e. These probabilities are given in Tables IV and V.

Tawde and Laud[31] calculated relative transition probabilities given in Table V independently of Pillow[46,47] by using the same "distortion" technique Pillow used in 1951. Their values agree with those of Pillow. They also found that values calculated with Hutchisson's integral are in better agreement with experimental data than those of the distortion technique. Tawde and Laud think that the anharmonicity introduced by the distortion makes the comparison between theory and experiment worse. The magnitude of the shift in the right direction is too much exaggerated. However, Pillow's 1953 calculation with the use of the same anharmonic approach for getting wave equations agrees with King's data, as well as does the Hutchisson method used by Tawde and Laud. Results are presented normalized within a given vibrational sequency, Δv = constant, so that the sum of the sequence is unity or

$$\sum_{v''} \left[\int \psi_{v'} \psi_{v''} \, dr \right]^2 = 1 \qquad (70)$$

because the electronic transition moment is assumed to be constant.

Tawde and Rajeswari[62] have made calculations comparing Hutchisson's method; a simple harmonic-oscillator approximation by using tables prepared by Bates;[63] a modified harmonic-oscillator method by applying first-order perturbation theory to find the anharmonicity correction to the wave functions; and the Morse approximation by using numerical intergration, as was used by Pillow and Tawde and Laud. The four methods give results which are in close agreement.

Fraser, Jarmain, and Nicholls[64] report arrays of overlap integrals for the C_2 Swan system shown in Table V. The vibrational wave functions were calculated by using two Morse potentials and one suitably-adjusted parameter. One potential is displaced from the other at equilibrium position. Solution of the Schroedinger wave equation gives vibrational wave functions. An improvement termed the "r_e shift" requires a systematic displacement of wave functions to compensate for one of the distortions introduced by the approximation.

Nicholls[65] evaluates the variation of the electronic-transition moment $R_e(r)$ as a function of r, by using King's experimental data for the integrated-band intensity for the C_2 Swan system. He reports smoothed arrays of relative transition probabilities. For the integrated intensity he uses

$$I_{v'v''} = KN_{v'}E^4_{v'v''}p_{v'v''} \quad , \qquad (71)$$

where K is a constant that allows for units and geometry. $N_{\nu'}$ is the number of molecules in the upper state. $E_{\nu'\nu''}$ is the vibrational transition probability for the band, defined by

$$p_{\nu'\nu''} = R_e\ (\bar{r}_{\nu'\nu''})\left|\int \psi_{\nu'}\psi_{\nu''}dr\right|^2 . \tag{72}$$

From the measured integrated intensity and $N_{\nu'}$, the $p_{\nu'\nu''}$'s for C_2 Swan bands were found. From the expression for $p_{\nu'\nu''}$, Eq. (72), the overlap integral $\int \psi_{\nu'}\psi_{\nu''}\ dr$ was calculated by using the Morse potential to obtain vibrational wave functions. Thus $R_e(\bar{r})$ could be found. The $\bar{r}$ centroid

$$\bar{r} = \frac{\int \psi_{\nu'}\ r\ \psi_{\nu''}\ dr}{\int \psi_{\nu'}\ \psi_{\nu''}\ dr} \tag{73}$$

was also calculated, and a plot of $R_e(\bar{r})$ as a function of $\bar{r}$ gave a constant straight line over a significant range of r, $1.17\mathring{A} < r < 1.62\mathring{A}$. Nicholls concluded that since $R_e(\bar{r})$ is a constant for the C_2 Swan system, then the Franck-Condon factors are a relatively reliable measure of the vibrational transition probability. He gives as the r variation, $R_e(\bar{r})$ = constant (1 + 0.056 r). Development of the method is reviewed by Nicholls.[66] Jarmain[67,68,69] has calculated, by computer, values of the Klein-Dunham potential-energy functions for several diatomic molecules including C_2 and CN, and compared the potential-energy to those obtained by using Morse potentials. He finds that the Klein-Dunham potential gives good agreement with experimental data. He plans to use the

tabulated "true" potential-energy functions in the Schroedinger equation to find more-accurate vibrational wave functions. Accurate wave equations would be useful in any theoretical calculation of oscillator strengths.

Two other groups, Singh and Jain[70] and Read and Vanderslice[71] have constructed true potential-energy curves for C_2, both using the Rydberg-Klein-Rees potential. Read and Vanderslice point out that their curves are in very good agreement with Jarmain's. All three computations give improved results compared to the Morse potential.

Coulson[72] has pointed out that quantum-mechanical theoretical calculations give reasonable estimates without too much trouble. He states further that the valence-bond and molecular-orbital methods are approximations by which a qualitative understanding of the bonding phenomena may be attained. Theoretical studies of C_2 have been valuable in establishing the important variables of the oscillator strength, the electronic transition moment, and the overlap intergral. To appreciate the useful subtleties of the proposed theories, however, a reliable experimental f value is needed for comparison.

Table I. Experimental relative transition probabilities of the Swan bands.

$v'v''$	λ (Å)	Johnson & Tawde mean of five measurements 1932	Tawde & Patel mean of five sets 1937
2,0	4382	0.04	0.11
3,1	4371	0.09	—
4,2	4369	0.17	—
1,0	4737	0.44	0.57
2,1	4715	0.56	0.61
3,2	4697	0.59	—
4,3	4684	0.66	—
5,4	4673	0.85	—
0,0	5165	1.00	1.00
1,1	5129	0.42	0.46
2,2	5097	0.12	0.21
3,3	5070	0.05	—
0,1	5635	0.46	0.46
1,2	5585	0.42	0.39
2,3	5540	0.44	0.43
3,4	5501	0.45	—
4,5		0.33	—
0,2	6191	0.32	0.18
1,3	6122	0.49	0.20
2,4	6059	0.63	0.26

Table I. continued: Experimental relative transition probabilities of the Swan bands.

$v'v''$	λ (Å)	Patel mean of four sets 1947	Tawde & Laud mean of four sets 1951
2,0	4382	0.09	0.04
3,1	4371	——	——
4,2	4365	——	——
1,0	4737	0.65	0.38
2,1	4715	0.65	0.55
3,2	4697	——	——
4,3	4684	——	——
5,4	4673	——	——
0,0	5165	1.00	1.00
1,1	5129	0.43	0.48
2,2	5097	0.22	0.20
3,3	5070	——	——
0,1	5635	0.59	0.35
1,2	5585	0.48	0.43
2,3	5540	0.43	0.46
3,4	5501	——	——
4,5		——	——
0,2	6191	0.24	0.10
1,3	6122	0.28	0.16
2,4	6059	0.48	0.19

Table II. Experimental relative transition probabilities of the Swan bands.

$v'v''$	λ (Å)	King King furnace 1948	Phillips King furnace 1954	Phillips King furnace 1957
2,0	4382	0.044	—	—
3,1	4371	0.111	—	—
4,2	4365	0.252	—	—
1,0	4737	0.358	0.362	0.298
2,1	4715	0.525	0.51	0.407
3,2	4697	0.718	0.76	—
4,3	4684	0.952	—	—
5,4	4673	1.56	—	—
0,0	5165	1.000	1.000	1.000
1,1	5129	0.520	0.64	0.470
2,2	5097	0.256	—	—
3,3	5070	—	—	—
0,1	5635	0.244	0.263	0.413
1,2	5585	0.470	0.37	0.529
2,3	5540	0.497	—	—
3,4	5501	0.802	—	—
4,5				
0,2	6191	0.043	—	—
1,3	6122	0.123	—	—
2,4	6059	0.188	—	—

Table III. Theoretical oscillator strengths of the Swan band system.

	f
Lyddane, Rogers, and Roach	0.024
Stephenson	0.029
Shull	0.13
Shull	0.18
Coulson and Lester	0.24
Clementi	0.0485

Table IV. Theoretical relative transition probabilities of the Swan bands.

$v'v''$	λ (Å)	McKellar & Buscombe Hutchisson integral 1949	Pillow 1951	Pillow 1951
2,0	4382	0.067	0.05	0.03
3,1	4371	0.149	0.20	0.10
4,2	4365	0.215	—	0.17
1,0	4737	0.324	0.46	0.30
2,1	4715	0.422	0.65	0.49
3,2	4697	0.392	0.67	0.57
4,3	4684	0.334	—	0.60
5,4	4673	—		
0,0	5165	1.000	1.00	1.00
1,1	5129	0.436	0.48	0.49
2,2	5097	0.144	0.23	0.23
3,3	5070	0.022	0.13	0.10
0,1	5635	0.354	0.15	0.26
1,2	5585	0.511	0.18	0.36
2,3	5540	0.544	0.17	0.32
3,4	5501	0.498	0.24	0.29
4,5		—	—	—
0,2	6191	0.048	0.36	0.06
1,3	6122	0.121	0.07	0.14
2,4	6059	0.203	0.10	0.23

Table IV. continued: Theoretical relative transition probabilities of the Swan bands.

$v'v''$	λ (Å)	Pillow 1953	Wyller 1953 WKB	Wyller 1953 WKB_n
2,0	4382	0.04	0.030	0.029
3,1	4371	0.11	0.115	0.111
4,2	4365	0.19	0.212	0.200
1,0	4737	0.32	0.345	0.336
2,1	4715	0.49	0.560	0.528
3,2	4697	0.59	0.622	0.565
4,3	4684	0.65	0.631	0.546
5,4	4673			
0,0	5165	1.00	1.000	1.000
1,1	5129	0.51	0.473	0.453
2,2	5097	0.24	0.174	0.160
3,3	5070	0.10	0.026	0.023
0,1	5635	0.31	0.313	0.310
1,2	5585	0.40	0.448	0.421
2,3	5540	0.38	0.415	0.376
3,4	5501	0.29	0.315	0.275
4,5		0.27		
0,2	6191	0.05	0.060	0.059
1,3	6122	0.13	0.152	0.146
2,4	6059	0.21	0.227	0.214

Table V. Theoretical relative transition probabilities of the Swan bands.

$v'v''$	λ (Å)	Tawde and Laud Hutchisson integral 1953	Tawde and Laud Old distortion 1953	Fraser, Jarmain, and Nicholls 1954
2,0	4382	0.05	0.05	0.033
3,1	4371	—	—	0.082
4,2	4365	—	—	0.133
1,0	4737	0.32	0.46	0.324
2,1	4715	0.41	0.65	0.487
3,2	4697	—	—	0.554
4,3	4684	—	—	0.584
5,4	4673	—	—	—
0,0	5165	1.00	1.00	1.000
1,1	5129	0.45	0.48	0.496
2,2	5097	0.16	0.23	0.222
3,3	5070	—	—	0.078
0,1	5635	0.33	0.15	0.289
1,2	5585	0.49	0.18	0.383
2,3	5540	0.53	0.17	0.383
3,4	5501	—	—	0.360
4,5		—	—	—
0,2	6191	0.04	0.36	0.057
1,3	6122	0.11	0.07	0.120
2,4	6059	0.19	0.10	0.170

EXPERIMENTAL EQUIPMENT

A. Furnace Description

A King-type graphite-resistance-tube furnace designed by W. M. Brower, which has been described by Brewer, Gilles, and Jenkins,[73] was used as a source for C_2 . Power was obtained by passing 440-V, 90-A, 60-cycle line power through 6-kW and 100-kW transformers, giving voltages at the furnace of 0 to 15 or 0 to 30 V and up to 2000 A, depending on the resistance of the graphite. Two 7.5-kW powerstats wired in parallel gave a fine control on the current. A reversing switch in the circuit connected in parallel to the 6-kW transformer provided for the reduction or increase of the current output at the furnace. The 110-line voltage could be used through the same circuit for much-lower temperatures and thus gave a total range of accessible temperatures of 600°C to 3000°C. The maximum temperature depended on the thickness and diameter of the graphite tube. Small-diameter tubes with thick tube walls made possible higher attainable temperatures before the tube burned out. The current was introduced from the circuit through the graphite tube by copper bus bars fitted tightly around copper blocks at either end of the furnace. One end of the inner copper-furnace spool support was grounded; the other was at the circuit potential. The graphite tube completed the circuit.

A spool-shaped piece of graphite that encircled the tube and held five layers of concentric cylindrical graphite radiation shields was supported by a metal structure. The spool was insulated from the

grounded outer tank by quartz rods that fastened one end of the spool into the disk cavity in one of the copper blocks. On the other end teflon was used to insulate the inner metal support from the outer chamber. Water through copper tubes cooled the inside metal support, the outer tank, and the windows. The cooling tubes were insulated from the ground potential of the water pipe by rubber connections. Difficulty was encountered with sudden increases in water pressure which split the heavy (1/4 in.-wall) rubber tubing until the inlet lines were wrapped along their entire length with friction tape.

The furnace could be evacuated with a forepump to less than 100 μ, as read on a Hastings thermocouple gage. At the ungrounded end of the furnace, a rubber o ring compressed by a threaded bakelite fitting against a bakelite ring on the inner copper support gave the insulated vacuum seal. At higher temperatures the rubber o ring hardened, and vacuum was lost. The bakelite fitting became smaller under the heat and would bind on the threads. C. D. Grandt of the physics machine shop designed a brass fitting with sticky teflon on the outer edge. The 1/8-in. space between the grounded furnace chamber and the teflon was sufficient insulation for the 15 to 20 V used in the furnace. The brass fitting gave a good vacuum-tight compression against a silicone rubber o ring, which did not harden except at the highest temperatures used with C_2. Valves provided for introduction of gases into the furnace; gas pressures were measured on a manometer. Quartz windows at either end of the furnace tube made possible the focusing of the hot zone on the spectrograph slit from one end, and the reading of the temperature with a Leeds and

Northrup optical pyrometer at the other end. The temperature was read either on a TaC plug at the center of the graphite tube or on the hottest part of the tube wall.

The removable windows described by Engelke[74] provided for removal and introduction of the graphite tube, which is supported by two conical split graphite bushings that make connection with the copper blocks at either end. The tubes similar to those described by Hicks[23] and Krikorian[75] had a 1/2-in. bore drilled uniformly through the length of the tube. A 6-in. heating zone in the center of the tube was machined with a tapering outside diameter from 0.865 in. at the center to 0.750 in. at the constrictions or points of minimum cross section, which are located 3-1/4 in. from either end. The outside diameter of these 3-1/4 in. sections was 0.877 in. The use of the tapered tubes counteracted the flow of heat out of the open ends of the heating zone by increasing the power output of the walls in these regions. Figure 8 gives a sketch of the tube.

To further define the hot zone, 1/4-in.-i.d., 1/2 in.-long baffles were placed at each end of the tapered region. The baffles also were used to reduce the amount of wall radiation reaching the spectrograph and to minimize diffusion of the gaseous species from the hot zone.

Focusing the King furnace on the 3-m concave-grating spectrograph was complicated by the presence of horizontal striations of the photographic plates when the plates were exposed to continuous radiation from or through the furnace. Some of the striations were of the type to be expected from the astigmatism of the concave grating. In this

case the image is more intense through an equatorial horizontal plane, and the intensity decreases on either side. Sawyer[76] points out that the astigmatism makes it impossible to photograph, for comparison, two spectra in juxtaposition by illuminating one portion of the slit with one light source and an adjacent portion with another.

In addition to the presence of astigmatism there were present intense striations alternating with weak-intensity striations. The slit was carefully examined and did not seem to be the source of the effect because the position on the plate and number of striations varied as the furnace distance from the slit, or the stops between the furnace and the slit were varied. Also the diameter of the tube, the presence of baffles in the tube, and the diameter of these baffles caused the striations to appear differently. The striations were eliminated by removing wall light and focusing a well-collimated beam onto the slit. The optics are given in Fig. 8, p. 64. Striations caused by the slit appeared when a very small slit (approx. 10 μ) was used. Also some of the tungsten lamps were inhomogeneous in intensity and gave striations when larger slits were used.

APPARATUS

B. Optical Pyrometer Calibration

Introduction

A disappearing-filament optical pyrometer is used for measuring the temperature of a TaC blackbody plug inside the King furnace. Planck's law with the two radiation constants c_1 and c_2 and the use of monochromatic radiation relates the 1948 International Temperature Scale to the thermodynamic scale. As reference point the freezing point of gold (adopted as 1063.00°C on the 1948 International Temperature Scale) is used. Lovejoy[77] reviews the standard deviation obtainable with a standard optical pyrometer and shows from extrapolated calibration data on tungsten lamps that it is 2°C at 2200°C and 4°C at 2800°C. He estimates that the standard deviation obtainable with a nonstandard pyrometer would be twice that of the standard type. The accuracy of the 1948 scale requires correcting by 1.7°C at the gold point, according to the recent determination of 1336.2°K as the freezing point of gold by Moser, Otto, and Thomas.[78]

Improvement in the value of c_2 reported by DuMond and Cohen[79] as 1.43884 cm deg gives a correction of 0° at the gold point and -5° at 4000°C. Current measurements then indicate the 1948 scale is low by 5°C at 2200°C and 6.5°C at 2800°C according to Lovejoy.

Method of calibration

To put the measured temperatures on a reproducible scale, the disappearing-filament optical pyrometer from Leeds and Northrup was

calibrated against a similar one that had been calibrated by the U.S. National Bureau of Standards. A tungsten lamp originally calibrated by General Electric Co. with a vertical filament of 2 by 50 mm was viewed just below a notched point by the two pyrometers set at 12.5° off the normal to the filament, to minimize reflections from the glass envelope of the lamp[80], and to make possible the sighting of the filament with both pyrometers. Interchanging the pyrometers had no effect on the observed temperature. The lamp was operated from six 6-V storage batteries wired in parallel to deliver 12 V. During operation the batteries were charged at a current rate just below the current in the lamp circuit to minimize drain on the batteries. The current in the circuit was obtained by reading the voltage with a potentiometer across a standard 0.01-Ω resistor. The temperature of the lamp could be varied by changing the number of resistors in series in a resistor box. Figure 1 illustrates the procedure.

For calibrations with the use of a blackbody plug in the King furnace, the pyrometers alternately were sighted into the furnace tube at the same end at a distance of approximately 90 cm from the plug. Care was taken to mount each pyrometer telescope in a reproducible way. The arrangement is shown in Fig. 2.

Treatment of data

The lamp was calibrated in the temperature range 1200 to 1700°C because the high and extra-high scales of the pyrometer are useful ones for current work. Three individuals took temperatures readings for the March 1962 calibration. These calibrations are compared with

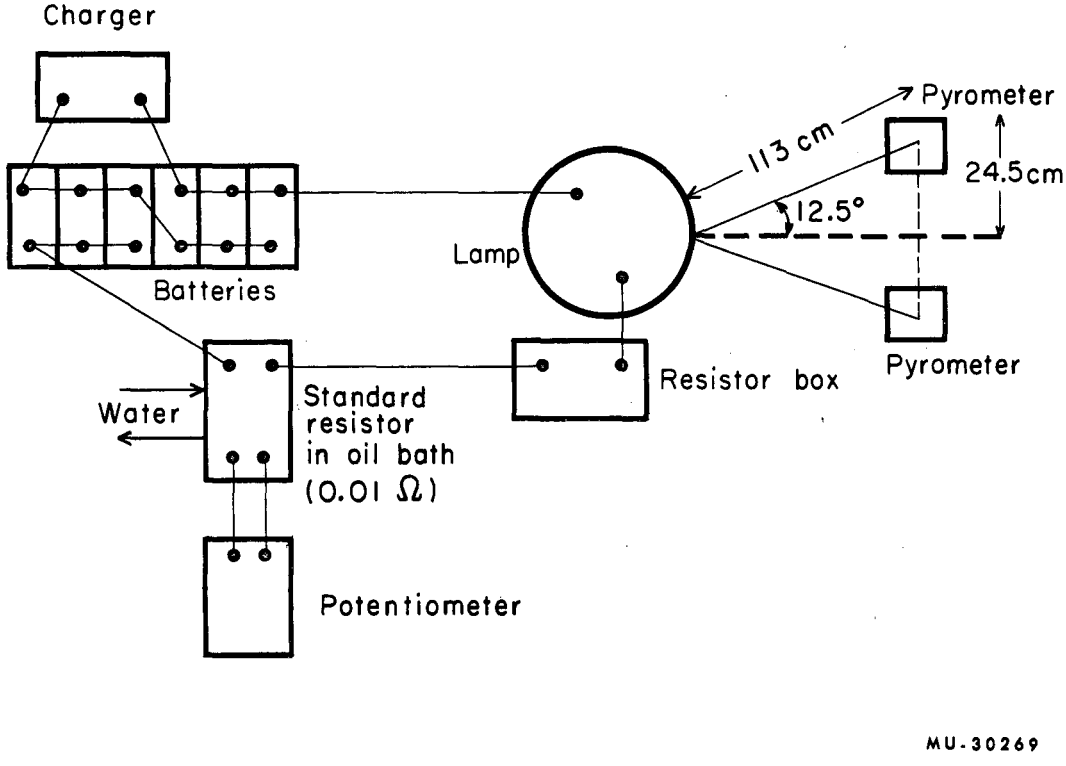

Fig. 1. Schematic diagram for calibration of optical pyrometer with tungsten lamp.

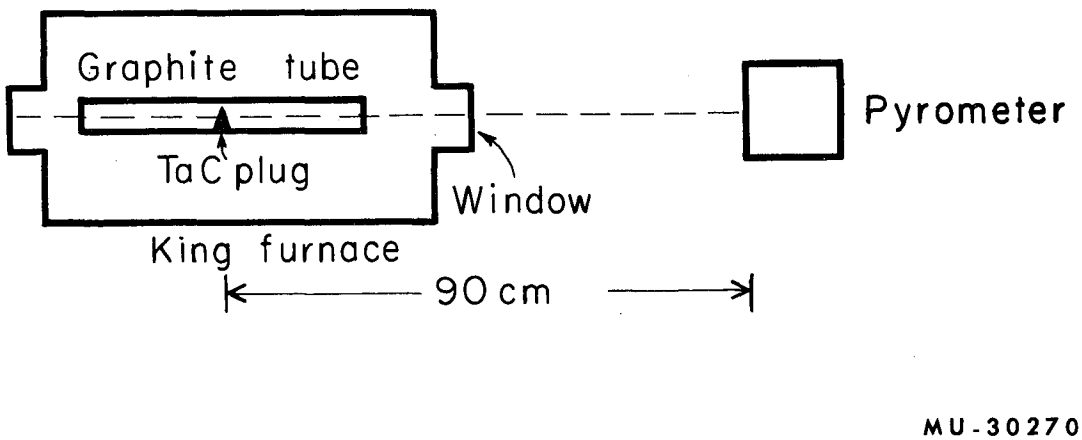

Fig. 2. Schematic diagram for calibration of optical pyrometer with King furnace.

measurements taken by one person in October 1961. Results are shown in Fig. 3. The differences between the calibration of the No. 2 pyrometer and the standardized pyrometer are found and averaged. For temperatures between 1200 and 1660°C the No. 2 pyrometer reads high by 14 to 16°C on the high scale. On the extra-high scale the pyrometer is high by 24 to 33°C. The No. 2 pyrometer printed scale is based on the 1927 International Scale whereas the standard one is based on the 1948 scale; this accounts for a high reading of 1 to 5°C for the range 1200 to 1800°C, and 8 to 13°C for 2200 to 2600°C.[81] The temperatures observed as a function of lamp current for the No. 2 pyrometer are also plotted in Fig. 3. The two calibrations are comparable except for a parallel displacement of the October 1961 data because of improper zeroing of the potentiometer. Previous calibrations of the lamp, including the General Electric calibration of 1946, and two calibrations in the Berkeley laboratory of March 1956 and May 1957 are included to show consistency of the calibration with respect to the lamp. The lamp calibration is used as an internal check only. The No. 2 pyrometer is compared directly with the pyrometer calibrated by the National Bureau of Standards in Washington.

The blackbody calibrations on the King furnace were made for the temperature range 1700 to 2350° by three observers over a period of three days. The temperatures within a day are consistent without appreciable variation between observers. Over the three days it was found that the average deviation was approximately 10° for 1700 to 2350°C. The observed temperatures as a function of current in the primary transformer circuit for the furnace are shown in Fig. 4.

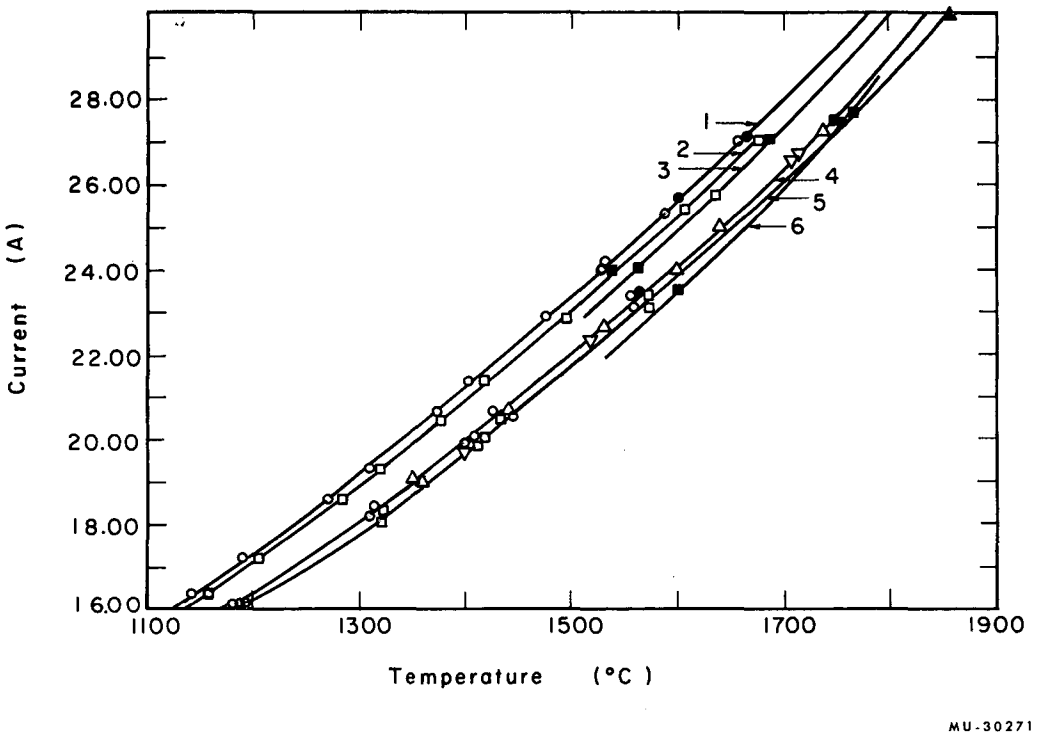

Fig. 3. Calibration of No. 2 pyrometer with 86-P-36 G. E. tungsten lamp:

Lamp calibration

▽ March 1956 calibration
and △ May 1957 calibration;
Oct. 1961 calibration, Curves 1, 2, and 3, and March 1962 calibration, Curves 4, 5, and 6.

Pyrometer calibration

○ Standard, H scale,
● Standard, xH scale,
□ No. 2, H scale,
■ No. 2, xH scale;

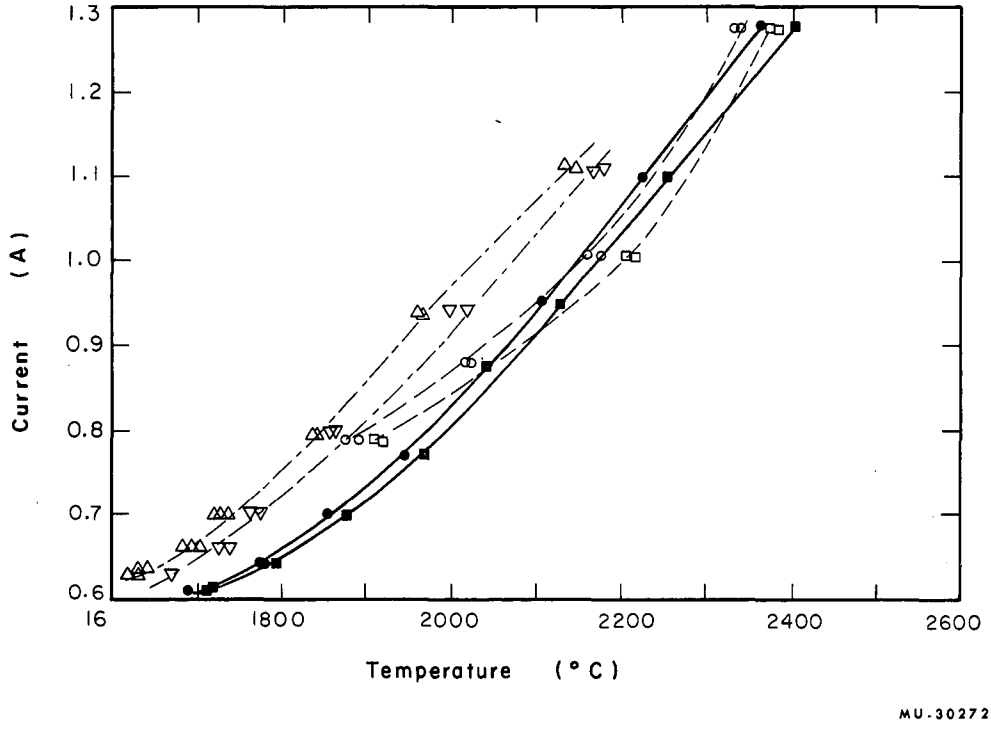

Fig. 4. Calibration of No. 2 pyrometer with King furnace for xH scale:

-.. - △	Standard	March 19, 1962,
-.. - ▽	No. 2	March 19, 1962;
--- ○	Standard	March 20, 1962,
--- □	No. 2	March 20, 1962;
—— ●	Standard	March 21, 1962,
—— ■	No. 2	March 21, 1962.

The resistance of the graphite tube changes as it is heated, and therefore the curves are displaced. However, the difference between the No. 2 and standard-pyrometer temperature readings is the value of interest. The corrections obtained from Fig. 3 and 4 are plotted in Fig. 5 against the temperature reading of the standard pyrometer.

To check the consistency of the calibration, the transmission of the filter, introduced in the optical-pyrometer optics when the extra-high scale is used, is calculated from the relation

$$\frac{1}{T_{H\ scale}} - \frac{1}{T_{xH\ scale}} = \text{Transmission} \qquad (74)$$

at constant-pyromter lamp current. Corrections to the No. 2 pyrometer scale were made by averaging the calibration corrections shown in Fig. 5, plotting these in Fig. 6, and interpolating between points. The first four points are extrapolated values for the high scale and measured values of the lamp and furnace for the extra-high scale; however, these values seem particularly inconsistent. The consistency of the two curves for the measured points indicated that the averaged corrections are reasonalbe.

For calculations involving temperature a correction of 40°C will be subtracted from the No. 2-pyrometer reading in the range of interest 2200 to 2600°C, to bring it in line with the standard and thus put the laboratory reading on the 1948 International Temperature Scale. From the furnace calibrations an accuracy of ±10°C may be assigned to the temperature. The error is partly due to the continually increasing temperature of the King furnace.

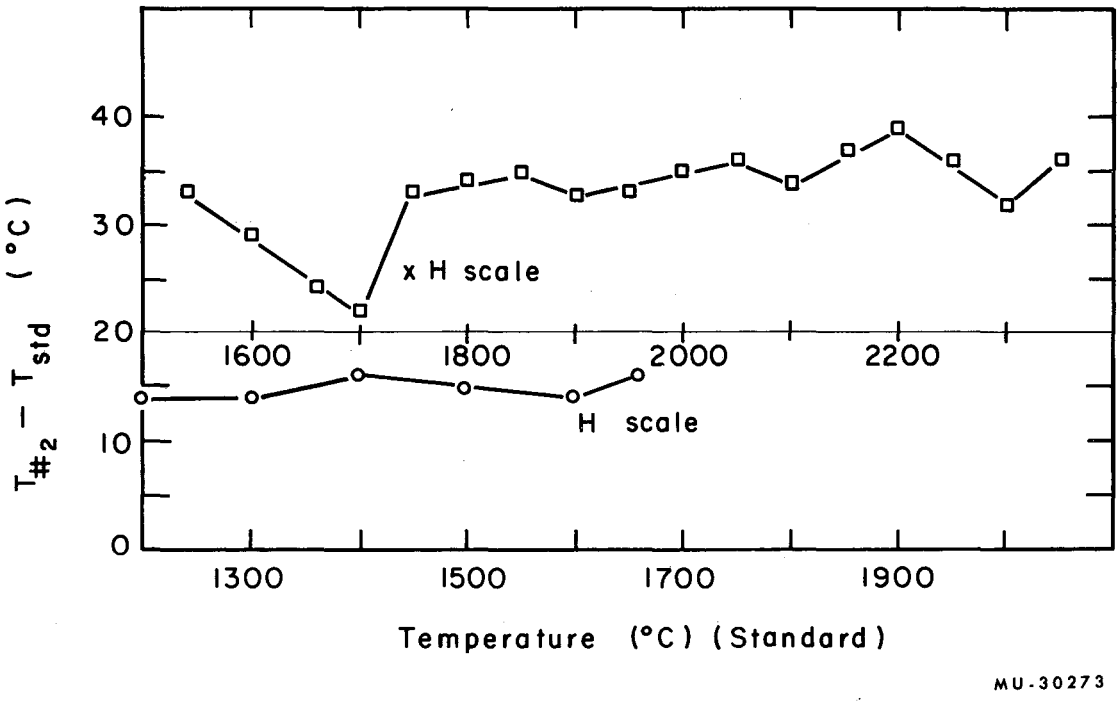

Fig. 5. Temperature differences between No. 2 and standard pyrometers.

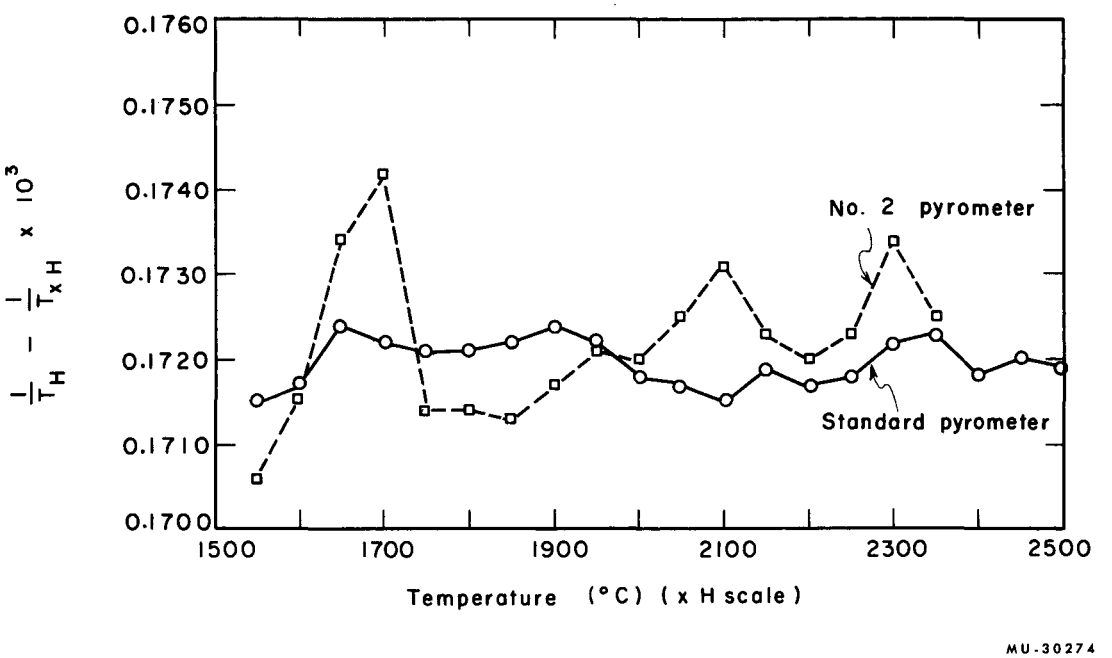

Fig. 6. Transmission of standard and No. 2 pyrometers by comparing H and xH scales.

A value of $5^{\circ}C$ should be added to the corrected optical-pyrometer reading in the range 2200 to $2600^{\circ}C$ to put the 1948 International Scale on the current thermodynamic scale. Unless indicated, however, the 1948 scale will be used.

C. Concave-Grating Spectrograph

A 3-m concave-grating spectrograph with Eagle mount was used in second order. The 3-in. by 5-in. grating with 15,000 lines per in. gave a plate factor of 2.76Å per mm. With a slit opening of 10 to 20 μ the lines of the General Electric G18T6 mercury germicidal lamp were broadened from theoretical width of 0.007Å given by Worden[82] to a width on the 3-m-grating spectrograph of 0.25Å to 0.50Å. To calculate the astigmatic broadening, the relation given by Sawyer[76] and by Beutler,[83]

$$z' = 2\ell \sin^2 \alpha - z \tag{75}$$

was used for the Eagle mount, where α (the angle of incidence to the grating) is equal to β (the angle of diffraction). Let z be the height of a source at the slit and ℓ be the length of the grooves of the grating, then z is the length of the images formed by a point light source at the slit.

For the experimental values

$$\ell = 76.2 \text{ mm},$$

$$\alpha = 16^\circ 47',$$

and $$z = 0.1 \text{ mm};$$

then z′ is 12.59 mm high. The point source is broadened to 12.69 mm at the plate. This astigmatic broadening is larger by an order of magnitude than broadening from coma, curvature, and aberration. The astigmatic broadening may be measured experimentally by placing a horizontal slit at the Sirk's position s for horizontal

focus, as given by Beutler:

$$s = R\left(\frac{1}{\cos\alpha - \sin\alpha \tan\alpha} - \cos\alpha \right), \qquad (76)$$

where R (of 300 cm) is the radius of the concave grating and α is $16^{\circ}47'$, the angle of incidence and diffraction of the source to the Eagle mounted grating. Then the Sirk's focus is located at 57.5 cm from the slit. To get a true measure of the astigmatic broadening, care must be taken that the grating length be filled with light from the source at the horizontal focus. Krikorian[75] by using a 0.1-mm-slit opening measured an image 0.6-mm high for z′ in first order. He concluded that 0.5 mm should be subtracted from his lines to correct for broadening. For the present experiments on C_2 there is justification then for using the measured half-widths of the narrow mercury-lamp lines and of the atomic-impurity lines in the furnace as instrumentally-broadened Doppler-shaped lines. Krikorian showed with interferometer experiments that Zr lines in the furnace were Doppler-shaped. Geometrical optics of the King furnace and 3-m grating are discussed in Appendix A.

To focus the spectrograph the spectral region was selected by changing the angle of the grating to the proper region, as determined from a light source with lines in the proper region. It was possible to use the 4358Å mercury line for the C_2 experiments. The line was examined visually in the plate position through an old developed photographic plate which had been scratched with a file to make the spectra partially visible.

A Bausch and Lomb eyepiece with a magnification of seven was used. The nominal plate tilt was fixed before this examination, at an angle near the exact angle of the grating. The best focus as determined by eye was then found by moving the grating and its marker along a meter stick toward or away from the photographic plate until the line was most narrow and equally intense along its length. Then the slit was moved in toward the grating or out to further refine the focus. Sometimes, then, the grating distance had to be readjusted. A photographic plate was then exposed for a series of grating-scale settings about 0.05 cm apart until the best grating-scale focus was determined. The slit was rotated to make it parallel to the grating lines. For this process it was most convenient to scan the lines. The rotation of the slit was not reproducible, and possibly some of the line broadening is due to nonparallel slit and grating lines.

D. Photographic Plates

Kodak photographic plates, 103a-F and IIa-F for C_2 were used. Plates were removed from the refrigerator and allowed to come to room temperature before opening, to prevent moisture from forming on the emulsion. Exposure times of 3 sec to 18 min were used. Equal time of exposure for the spectra and calibrated-step weakener was used. Calibrations were made by using a General Electric tungsten lamp connected to lead storage batteries. Plates were developed within 30 min to 1 h after the last exposure, in Kodak D-19 developer for 4 min for 103a plates and in Kodak D-76 developer for 15 min for IIa plates. During development the plates were lightly brushed with cotton to minimize the Eberhard effect. The plates were then rinsed for 30 sec and placed in Kodak Rapid Fixer for 5 min. The temperature of solutions was approximately 20°C. Then the plates were rinsed for 30 min to 1 h in running water. Plates were removed from rinse, wiped with chamois cloth, and dried for at least 12 h at room temperature away from drafts before scanning. The IIa plates were found to give a linear relation between exposure time and intensity, and had smaller-grain size than the 103a plates. They were two to three times slower.

E. Instrumentation

The equipment used for scanning the spectra consisted of a Cary Model 31, Serial 1074 vibrating-reed electrometer with a 9-position-selector range of 1 mV to 30 V, a Leeds and Northrup 0 to 10 mV recorder, a 2-kV, 12-mA regulated dc power supply from the Lawrence Radiation Laboratory for the 1P21 photomultiplier tube, a General Electric synchronous scanning motor, and sets of gears which could be interchanged to vary the scanning speed. The scanning system has been described by Phillips.[84]

The electrometer[85] can measure currents that originate in a high impedance (10^7 Ω or higher) source as small as 1.0×10^{-17}A. The detection of current is accomplished by measuring the potential difference across a high-value-input resistor. A Victoreen 10^8-Ω resistor in a metal holder was used. The vibrating reed refers to the input-signal modulator, which is a special capacitor consisting of one stationary and one vibrating plate. The latter, called the reed, is moved through a predetermined distance by an electromagnet at a constant frequency, to create a cyclically varying capacitor.

The input signal across the 10^8-Ω resistor goes to the preamplifier which is a dc coupled amplifier with dc feedback to the screen grid of one of the two matched tubes for bias control. A band width of aobut 70 cps is provided. From the reed in the preamplifier the signal, modulated at 450 cps, is amplified and rectified in the amplifier and fed into the recorder. With an

input resistor the amplifier has a time constant of 0.01 and noise of 2×10^{-13} A. Drift is less than 0.004 mV/sec. If care is taken to use matched tubes for replacements, the amplifier is stable and is a reliable component.

The power supply had a stability of 0.05 to 0.1% at 900 to 1000V which proved to be sufficient because interchanging with a more-stable supply (0.01%) gave no change in stability of the system.

For the small signals from the C_2 rotational lines, difficulty from noise in the 1P21 photomultiplier tube and base interfered with measurement. The approximately 60-cycle noise was found to be due to corona discharge at the base of the plug when high voltages of 900 to 1000V were applied. Potting the resistor-divider string in silicone rubber compounds proved of no value. It was suggested by Dr. Beat Meyer of our research group to pot the base in epoxy resin. The potting technique developed was to use a mold around the base of resistors, pour in the epoxy, and allow to harden without the use of vacuum to remove air bubbles. The pin holes of the tube plug and mold were coated with silicone grease to prevent adherence. The epoxy that did harden in the pin holes was drilled out. Epoxy C-3 from Armstrong Products Company was used. The major problems were that the heat evolved from the resin during hardening and melted the insulation on the input high-voltage and signal leads which are side by side on the tube base. They became partially shorted and high voltage appeared on the signal. If the resistors and pin leads were not fully immersed

in the resin, the noise remained. However, it was possible to make two tube bases that were satisfactory. The base wiring is shown in Fig. 7.

Resistors were 1/4-W, 1-MΩ evaporated metal film. The first tube base was used with a 1P21 tube to scan the emission spectra, which was used for the f value determination. Cooling the tube and base with dry ice eliminated noise that sometimes appeared. Unfortunately, cooling caused the epoxy to crack, and the high-voltage and signal wires became shorted. Another base was made and used with the 1P21 tube and narrow-band pass (100Å) interference filters to monitor the temperature of the King furnace by measuring the intensity of the heads of C_2 at 5165Å and of CN at 3883Å. If the intensity of the feature of interest did not change on the monitor during photographic measurement, then it could be concluded that the temperature of the furnace remained constant. With this second base there was no noise or dark current on the tube at 900 V. When on foggy days noise did appear owing to base leakage of the tube, a drying agent in the base shield box eliminated the noise on all scales of the amplifier, 1 mV to 30 V, corresponding to current of less than 1×10^{-11} A on the 1-mV scale used for scanning the rotational spectra. To prevent leakage of the high voltage to the signal the base plug was split with a saw between the signal and high voltage pins.

Because of the difficulty in making a base without shorting the signal, it is apparent that the 1P21 photomultiplier tube

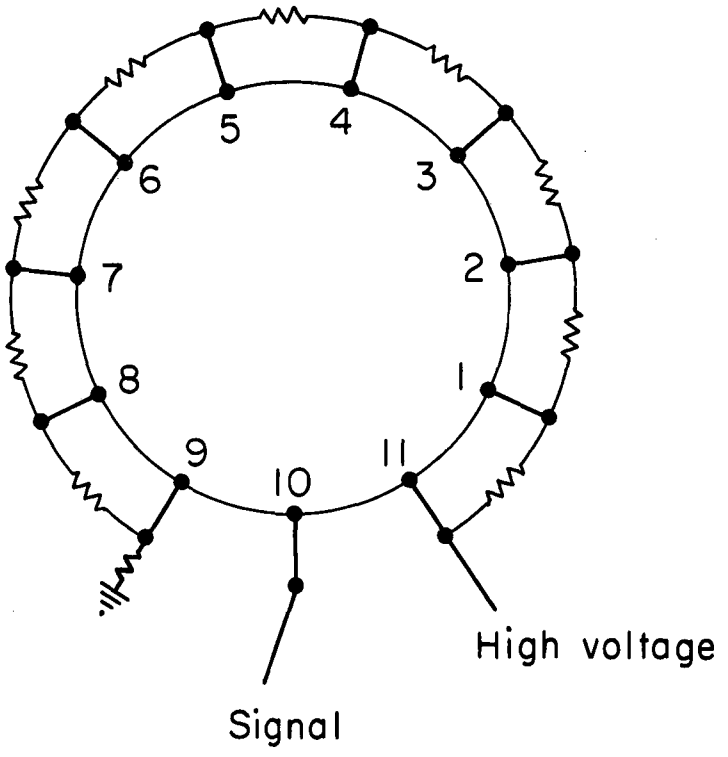

MU-30275

Fig. 7. Wiring for photomultiplier tube base (1-MΩ resistors).

would be more useful if the signal pin were put on top of the tube away from the high-voltage-supply circuit at the base.

EXPERIMENTAL PROCEDURE

The absolute intensity of the 0-0 Swan band ($^3\Pi_u$ - $^3\Pi_g$) of C_2 at 5165Å was measured in emission and absorption. In emission both the peak intensity of the head and the integrated intensities of rotational lines K'_P = 43 or 45 and K'_R = 16 or 18 were used to determine band intensity. It was possible to measure in absorption only peak-height intensity of the head. The optics for the measurement included an optical bench running under the furnace on a table and extending to the spectrograph slit, a 23-cm focal-length lens (A) near the furnace window, a camera shutter of 2- to 3-mm diameter to define the aperture, and a 6-cm focal-length cylindrical lens (G) at its focal length from the 10- to 20-μ slit. To further define the beam of light from the furnace, 1/4-in. stops (C), two at each end, were placed inside the furnace just behind the quartz windows (B). These stops prevented most of the background-wall radiation from the 1/2-in.-id tube from going through the beam to the detector. The two diaphragms near the back window helped prevent reflections that remained after tilting the window. For absorption experiments a vertical-strip-filament tungsten lamp with a 6-cm focal-length lens (F) mounted behind the furnace chamber were used to send parallel light through the furnace. Figure 8 presents a diagram of the optical arrangement.

The spherical lens (A) was focused near the back of the furnace to exclude wall light from the beam. The shutter stop was placed at the focus of this lens. The 2-in. by 5-in. concave grating with 15,000 lines per inch was filled with light and used in second order. The plate factor in second order is 2.7 to 2.8Å/mm.

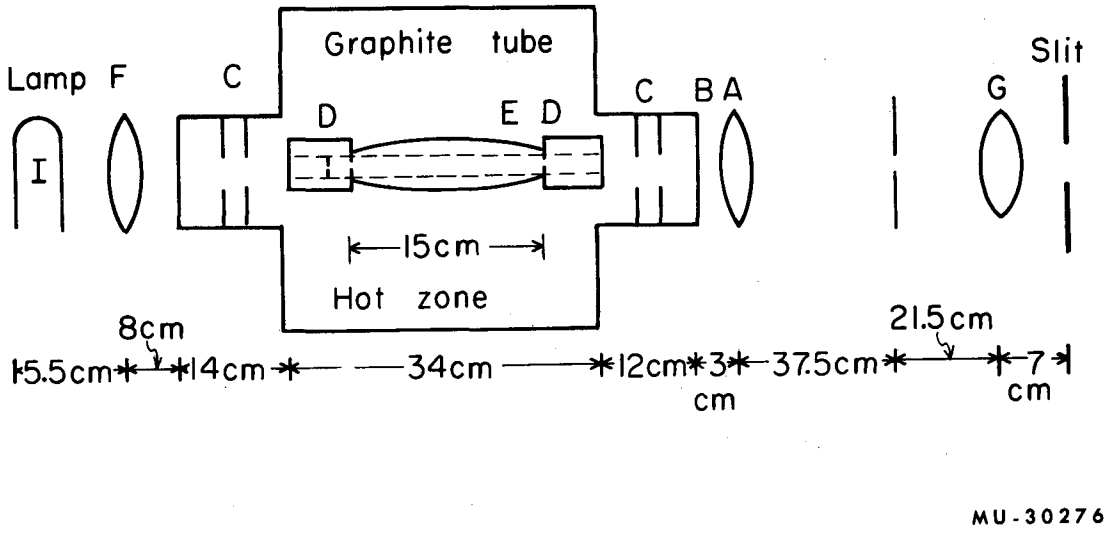

Fig. 8. Schematic diagram for optical arrangement for focusing gas on 3-m grating spectrograph: A, 23-cm focal-length lens; B, quartz windows of furnace; C, 1/4-in. -i. d. stops inside furnace chamber; D, 1/4-in. -i. d. graphite baffles inside graphite tube; E, TaC plug; F, 6-cm focal-length lens; and G, 7-cm focal-length cylindrical lens.

To define the hot zone (tapered 15-cm region) of the graphite tube, 1/4-in.-id graphite baffles (D) were placed in the tube. An additional baffle was used in the front of the tube to reduce the amount of wall radiation leaving the tube. For emission experiments a TaC plug (E) was used as a blackbody reference and was sighted on with a Leeds and Northrup optical pyrometer to read the temperature.

Emission measurements were made with 103a-F photographic plates. The circular image on the shutter appeared as a black region of gas with a key-hole blackbody region from the plug. Moving the lens (A) vertically placed the gas, then the blackbody on the shutter opening. First the spectra were photographed, then the plate was moved and lens (A) was adjusted so that only the blackbody light from the plug went through the optical train. Then by using Kodak neutral-density gelatin filters with the blackbody light, the blackbody reference light was exposed to the photographic plate for the same length of time as the spectral light. For absorption experiments with the use of the smaller-grained IIa-F plates, reciprocity of time and intensity was good and exposures of equal time were not a necessity.

Metal-film filters from Optics Technology were used because they have a constant optical density in the 4000 to 5000Å region. These filters gave white-light fringes.[86] Measurement of the distance between fringes, 0.25 mm, corresponded to 0.69Å. The distance between the film and outer part of the glass cover was calculated to be 1.8 mm compared to a measured distance of 1.5mm. By using the equation, $d = \frac{\lambda^2}{\Delta\lambda}$, at 5000Å, the filter therefore acts as an interferometer. Kodak gelatin filters that give no fringes were used, therefore, and their optical density in the region 3800Å to 6000Å was measured on a Cary Recording

Spectrophotometer Model 11, Serial 4.

It was first attempted to move a divider, and photograph different parts of the grating for spectral and blackbody exposures. However, the divider positions were not equivalent. Then the plates were cut along the 18-in. horizontal dimension to 1-3/4-in. to allow the plate to be moved in its holder for two exposures. For the absorption experiments C. D. Grandt and M. C. Yannke, machinists in the Physics Shop, devised a method for moving the plate in steps for five exposures on the 2-in. dimension of the 2-in. by 18-in. photographic plates.

The IIa-F plates were used, as were the 103a-F plates, for absorption of the 0-0 C_2 band in an attempt to make the very-weak absorption at the 0-0 head measurable on the Leeds and Northrup Recording Microphotometer, (Cat. No. 6700-P-1, Serial No. 1029390) connected with a Moseley Autograf Curve Follower. The microphotometer records variations in density of photographic plates driven at a uniform speed past a scanning device, which consists of an optical system containing a lead-sulfide photocell and a tungsten lamp with optically polished windows. The input from the microphotometer phototube was applied to the X axis of the recorder and Y as a linear function of X was led through the output potentiometer connection to the Leeds and Northrup Speedomax recorder. The curve-follower pickup coil followed a linear section of a metallic-ink graph. The Autograf increased the sensitivity of the electronic system so that it was possible to scan the weak absorption features of C_2. With the IIa-F plates the measurement error remained large, but the absorption line was more-clearly resolved visually.

To relate plate-darkening to intensity, a calibrated-step weakener

from Jarrell Ash Company in optical-density steps of 0.0, 0.215, 0.413, 0.606, 0.801, 1.000, and 1.208 was mounted on the spectrograph just behind the plate. The calibration was constant, within a 100Å region near the feature of interest.

At the high temperatures required for C_2 measurements the graphite tubes quickly developed gradients. Hicks[23] discussed similar problems with hot spots in the graphite tubes. Considerable time was spent machining the tubes to different dimensions, developing more efficient cooling, and altering the radiation shielding. A tube that gave a constant temperature along its profile at 2500°C developed a gradient at the higher temperatures. Each tube seemed to have a different temperature profile, for none of the tube dimensions tried gave a set of tubes with constant temperature in the hot region. The tubes burned out on the ground end of the applied potential of 15 to 20 V. Changing the water-cooling caused the tubes to last longer but did not prevent their burn-out at the same end. Reversing the tube in the furnace after it had been heated for an hour or two and cooled helped to lengthen the life of the tube, and caused more homogeneous heating in the hot zone until another gradient developed in about an hour.

For absorption experiments a tungsten lamp was used as absorber and photographed at different temperatures through the hot furnace. To further determine the temperature in the hot zone of the graphite tube in the presence of hot spots, the spectra were photographed in reversal. The reversal temperature defined as the temperature of the gas at 5165Å was the temperature at which the absorption exactly canceled out the emission. To obtain the reversal temperature, the measured brightness

temperature of the lamp at the reversal point was used to find the brightness temperature of the lamp at 5165Å from the relation.

$$\lambda_1 \ln\epsilon_1 - \lambda_2 \ln\epsilon_2 = \frac{hc}{k}\left(\frac{1}{T_2} - \frac{1}{T_1}\right), \qquad (77)$$

where λ_1 is 6530Å, ϵ_1 the emissivity of the tungsten filament at 6530Å, and T_1 the measured brightness temperature of the lamp; λ_2, ϵ_2, and T_2 refer to 5165Å; $\frac{hc}{k}$ is the second radiation constant. Emissivity values were estimated from De Vos' graph.[87] Five to ten exposures with the lamp at different temperatures gave the C_2 0-0 bandhead in absorption and emission. By comparing the different exposures on the plates and knowing the temperatures of the lamp, the reversal temperature could be determined within 20 to 50°C. At low temperatures the reversal temperature was not the same as the hottest part of the wall. At about 3000°K the hottest spot and reversal temperature were the same at the beginning of the experiment, but the hot spot in the tube became hotter than the reversal temperature in about an hour.

For some of the emission measurements the rotational lines used are given in Table VI; the wave lengths at which they occur are taken from Johnson.[88] The emission lines were scanned by using the same optics with a 1P21 phototube at the rate of 2.4A per min, slit openings of 100μ and by using the most sensitive 1-mV scale and a 10^8-Ω resistor to detect signals from the photomultiplier of less than 5×10^{-12} A. The electronic equipment has been described. It was not feasible to scan the absorption features.

TABLE VI. Rotational lines of 0-0 Swan band.

K'	λ(Å)
$P_3(43)$	5135.672
$P_{12}(43)$	5135.561
$P_3(45)$	5131.675
$P_{12}(45)$	5131.573
$R_3(16)$	5136.640
$R_{12}(16)$	5136.426
$R_3(18)$	5132.681
$R_{12}(18)$	5132.481

ANALYSIS OF DATA

For emission experiments on rotational lines the ratio of the integrated rotational-line intensity to the peak blackbody intensity was measured. The actual area of the blended lines was measured; the area was divided into area P(43) and area R(16), or P(45) and R(18) by multiplying by the percent populations of the P and R rotational levels. The area for a P or R line was then divided by three to get the area of each triplet. By assuming that in the absence of instrumental broadening each triplet is Doppler-broadened, the blackbody peak is treated as a triangle of the Doppler width. The resulting ratio $\frac{I_{K'}}{I_{BB}}$ is converted to $I_{K'}$ in absolute units by calculating I_{BB} independently from Eq. (7). The intensity, $I_{K'}$ or $I^{u\ell}$ in units of quanta per cm^2 per sec is substituted in Eq. (36) to obtain the intensity of a band I_{band}. For the value of the population ratio of K' to the band, the Boltzman ratio for a Doppler-broadened line

$$\frac{S_{K'}\, e^{-\frac{F'}{kT}}}{Q^{u}_{rot}} \tag{78}$$

was used. The f value is found by substitution into Eq. (37), where $\frac{I^{u\ell}(J' = a \text{ to } J' = b)}{I_{BB}}$ is R_o, the measured quantity, and

$$f = \frac{mc\,\lambda^2}{2\pi e^2 N'_o \ell} \cdot \frac{R_o I_{BB}}{\frac{\lambda_o^3}{c^3} \sum_{J'=a}^{b} S_{J'} \frac{c^3}{\lambda^3} e^{-\frac{F'}{kT}}} \Delta\nu \tag{79}$$

For these emission experiments, f for the C_2 0-0 Swan band is 0.004 ± 0.0007 for the scanning experiments, or 0.006 ± 0.004 for measurements on

103a-F photographic plates.

For the measurements on the 0-0 head, the ratio (the peak intensity of absorption or emission at the head to the lamp-peak intensity) was measured. These measured ratios in absorption were corrected for emission, which reduced the amount of absorption. For reversal conditions,

$$I_{abs}^{net} = 0 = I_{abs}^{lamp} - I_{em} + I_{abs}^{self} \quad , \tag{80}$$

where I_{abs}^{net} is the observed absorption, I_{abs}^{lamp} is the absorption of intensity from the lamp by the gas molecules in the lower state, I_{em} is the intensity of emission of gas molecules in the upper state, and I_{abs}^{self} is the self-absorption of the emitted light by the molecules. The measured ratios are

$$\frac{I_{abs}^{net}}{I_{lamp}} = a \tag{81}$$

and

$$\frac{I_{abs}^{lamp}}{I_{lamp}} = \alpha \ , \tag{82}$$

where I_{lamp} is the intensity of the lamp at the temperature of the lamp. The ratio α represents the fraction absorbed in the absence of emission or self-absorption. Substituting the definitions into Eq. (80) gives for the measured ratio

$$\frac{I_{abs}^{net}}{I_{lamp}} = \alpha \left(1 - \frac{I_{lamp}^{rev}}{I_{lamp}} \right), \tag{83}$$

where I_{lamp}^{rev} is the intensity of the lamp at the reversal temperature. Similar treatment gives for the measured emission ratio

$$\frac{I_{em}^{net}}{I_{lamp}} = \alpha\left(\frac{I_{lamp}^{rev}}{I_{lamp}} - 1\right) \quad . \tag{84}$$

Measured absorption ratios were less than corrected ratios by about a factor of two. Measured emission ratios were overcorrected by this technique. The ratio

$$\frac{I_{abs}^{net}}{I_{lamp}}$$

at low lamp temperatures was negligible compared to

$$\frac{I_{em}^{net}}{I_{lamp}} \quad .$$

The absorption ratios α were further corrected because one assumes for Eq. (19) a linear relation between population N'' and intensity. Thus,

$$\alpha = \frac{I_o - I}{I_o} = 1 - e^{-kC'} . \tag{85}$$

An expansion of C' equal to KN''ℓ in terms of α corrects for being off the linear curve of growth:

$$C' = \alpha + \frac{\alpha^2}{2} + \frac{\alpha^3}{3} + \frac{\alpha^4}{4} + \ldots\ldots \tag{86}$$

For small α, $C' = \alpha$.

The ratio for determining contribution of the measured rotational lines

$$\frac{\sum_{K'=a}^{K'=b} S_{K'} e^{-\frac{F'}{kT}}}{Q_{rot}^{u}} \tag{87}$$

was determined by plotting the lines with relative peaks fixed by the Boltzman relation but with a rotational line width of 0.25Å and of 0.50Å. This broadening was found by measuring half widths of very narrow (approx. 0.01Å) mercury lines from the General Electric G18T6 germicidal lamp and half widths of atomic impurity lines, with the assumption that they were Doppler-broadened, on the 3-m-grating spectrograph. Doppler broadening of rotational lines seems justified since Krikorian[75] found the atomic lines of Zr were Doppler-shaped by using an interferometric technique. He found no serious pressure broadening for Zr or C_2. Pressure broadening was calculated from the relation given by Mitchell and Zemansky,[3]

$$\Delta\nu = \frac{2}{\pi}\alpha^2 \frac{p}{RT} N \left[2\pi RT\left(\frac{1}{M_1} + \frac{1}{M_2}\right)\right]^{\frac{1}{2}} \tag{88}$$

where α^2, the effective cross section for Lorentz broadening, was used as 8.1×10^{-16} cm^2, N is Avagadro's number, p the pressure of foreign gas was taken as 10 cm, T as 2800°K, M_1 as 24.02 for C_2, and M_2 as 39.98 for Ar atoms. The broadening for 10-cm gas pressure is 0.02 cm^{-1} compared to a Doppler width of 0.15 cm^{-1}. The broadening of the lines due to astigmatism of the concave grating is discussed in the section on experimental equipment. The broadened lines resulted in a lower peak height, and the factor

$$\frac{\sum_{K'=a}^{K'=b} S_{K'}\, e^{\frac{-F}{kT}}}{Q^u_{rot}\ \Delta\lambda_i}, \tag{89}$$

where $\Delta\lambda_i$ is the instrumental half width, was considered equivalent to

the measured peak height. The value of this factor, determined from the graphical plot of rotational lines at the head with a half-width of 1 cm^{-1}, is 0.018. The error introduced here is of the order of a factor of two. It was assumed that the factor would be the same within less than a factor of two for the upper and lower states of the transition. Division of k by the Eq. (89) gave $\frac{I_{band}}{I_{lamp}}$. For absorption experiments this ratio was used directly to determine the f value of the band as 0.005 ± 0.003. For emission experiments the ratio, a, was used instead of k. The intensity of the band was found by multiplying the ratio by the intensity of the lamp at the measured temperatures corrected to 5165Å. The f value for absorption was calculated by substituting into Eq. (42) the measured and corrected ratio C' to give

$$f = \frac{mc}{\pi e^2 N_0'' \ell} \frac{C'}{\sum_{J''=a}^{J'=b} S_{J''} e^{-\frac{F''}{kT}}} . \tag{90}$$

The f values for emission experiments were calculated from Eq. (79). The f value for the 0-0 band for emission experiments at the head is 0.007 ± 0.004.

The rotational numbering in the head was determined from Johnson's[88] measurements and Budo's analysis of Johnson's data.[89] The wave-number positions of lines in the head were calculated from the relation

$$\nu_i = \nu_0 + (B'_\gamma + B''_\gamma)\, m + (B'_\gamma - B''_\gamma)\, m^2, \tag{91}$$

where ν_i is the wave number of interest, ν_0 is the zero line wave number of 19378.44 cm^{-1} given by Phillips,[90] and B'_0, B''_0 are the rotational

constants for the zero levels of the upper and lower states respectively. Values used are those Budo gives: $B_0' = 1.7452\ cm^{-1}$, $B_0'' = 1.6239\ cm^{-1}$. For the correct absolute numbering of the rotational levels, Budo's analysis of Johnson's data and Phillips' calculation from Budo's difference values of wave numbers for the J levels were compared.

Phillips points out that for the quantum number J = (K+1), K, or (K-1) correspond the subbands which are inverted in C_2: $^3\Pi_2 - {}^3\Pi_2$, $^3\Pi_1 - {}^3\Pi_1$, and $^3\Pi_0 - {}^3\Pi_0$, the red, central, and violet components of the triplets, respectively. For the 0-0 band of C_2 a comparison of Phillips' wave-number calculations from Budo's differences shows that K'' rather than J'' is the good quantum number because K'' numbering places triplets of the same K'' number together. Budo's numbering does not agree with Johnson's, but Shea, who also measured and analyzed the 0-0 band of C_2 but resolved only two of the three P triplets, points out that Johnson used a graphical method of analysis which gives inaccurate relative rotational numbering. Shea's relative numbering is correct. For Johnson's j-numbering the correspondence was used: K'' = j-1 for the P branch, and K'' = j-2 for the R branch. For Shea's j numbering the correspondence K'' = j-1 was used for both the P and R branches. Budo's J is equivalent to K. For the calculations of positions from Eq. (91) of rotational lines, $K_P'' = 1$ to 13; Johnson's data was fitted from $K_P'' = 14$ at the head. Since the blended head was used in the measurements and calculations of f values, the above calculation does not alter the results significantly. For the emission experiments on $K_P' = 43$ or 45, and $K_R' = 16$ or 18 the numbering is important.

The ratio $\frac{I_K}{I_{Band}}$ is defined in Eq. (35). The ratio for $K_P' = 43$ or 45

is approximately 0.0075 and for $K_R' = 16$ or 18 it is 0.01 for all temperatures used. Of course, in the calculations the exact values were used for the ratios. Rotational degeneracy S_K was calculated from equations summarized in Herzberg.[4]

The populations in the lower and upper states were calculated by using the free-energy function for a $^3\Pi$ state of C_2. Hence

$$\bar{F}^0 - \bar{H}_0^0 = 7.283 - \frac{3}{2} R \ln M - \frac{5}{2} R \ln T - R \ln 3 \tag{92}$$

$$= -4.377 - 11.439 \log T, \tag{93}$$

where R is the gas constant, M is the molecular weight of C_2(24.02) and T is the corrected temperature of the gas. The factor, $R \ln 3$, corrects for the degeneracy of the state, $^3\Pi_u$ or $^3\Pi_g$. The degeneracy, 3, for the $^3\Pi_u$ and $^3\Pi_g$ states is obtained by multiplying the partition function, Q_{rot}, by three to account for spin multiplicity and then by two because of lambda doubling, and dividing the product by two because C_2 is a homonuclear molecule and half the levels are missing.

Free-energy functions for solid graphite were taken from Pitzer and Clementi.[91] The heat of formation of the state, $^3\Pi_u(v'' = 0, K'' = 0)$, is 196.7 kcal/mole reported by Brewer, Hicks and Krikorian.[92] From the equation

$$\frac{\Delta F}{T} = \left(\frac{\bar{F}_T^0 - \bar{H}_0^0}{T}\right)_{gas} - 2\left(\frac{F_T^0 - H_0^0}{T}\right)_{graphite} + \frac{\Delta H_0}{T} = -R \ln P_{C_2} \tag{94}$$

representing the reaction, $2C_{(graphite)} = C_{2(g)}$, pressures of C_2 in the state $^3\Pi_g(v'' = 0, K'' = 0)$ were obtained. Molecules per cm^3, N_0'', in this level were obtained by use of the gas law,

$$N_o'' = \frac{PN}{RT} \tag{95}$$

where N is Avagadro's number and R is in units, cc atm per deg mole. For the upper state, $^3\Pi_g(\nu' = 0, K' = 0)$, the excitation energy for the transition $^3\Pi_g(\nu' = 0, K' = 0) \longrightarrow {}^3\Pi_u(\nu'' = 0, K'' = 0)$ of 55.4 kcal per mole was added to ΔH_0^0 for $^3\Pi_u$ to give ΔH_0^0 for $^3\Pi_g(\nu' = 0, K' = 0)$ of 252.1 kcal mole. Populations were calculated at 100° intervals from $2700^\circ K$ to $3200^\circ K$. Values between the intervals were interpolated. For populations at the higher temperatures where free energy functions are not tabulated, the term

$$\left(\frac{\overline{F}_T^0 - \overline{H}_0^0}{T}\right)_{gas} - 2\left(\frac{F_T^0 - H_0^0}{T}\right)_{graphite} \tag{96}$$

was plotted as a function of temperature and extrapolated to the higher temperatures.

Because of the gradients in the hot zone of the tube, there is some ambiguity as to the value ℓ, the length of the emitting or absorbing column of gas. The machined length of the hot zone was 15 cm; however, the temperature gradient at each end of the hot zone, as indicated by the gradient between the outer and inner faces of the baffles, would signify that perhaps one cm at each end should be subtracted and would result in ℓ of 13 cm for the hot zone. In the reversal experiments, the reversal temperature T_R gave the actual temperature of the gas.

To approximate the errors relative to tube length, consider a gradient in the tube. Let 5 cm of the tube be at a higher temperature T_2 than 10 cm at a lower temperature. Let $\ell_{T_1} + \ell_{T_2}$ equal 15 cm, and let ℓ_{T_R} equal 15 cm. Then if the equivalence

$$N_{T_1} \ell_{T_1} + N_{T_2} \ell_{T_2} = N_{T_R} \ell_{T_R} \tag{97}$$

is made, N_{T_R} may be calculated as a parameter, where N_T are the populations of C_2 gas at the defined temperatures. Table VII gives T_R calculated for temperature gradients of 100°, 200°, and 300°.

TABLE VII. Calculated reversal temperatures for assumed gradients in King-furnace graphite tube.

T_1	T_2	T_R
2900°K	3000°K	2933°K
2900	3100	3010
2800	3100	3000

From this combination of numbers it is apparent that the reversal temperature is nearer the higher temperature for 300° gradients and nearer the lower temperature for 100° gradients. For the 200° gradients the reversal temperature is intermediate. For the t-value calculations the value of ℓ used is 10 cm with an estimated variation, $\pm$ 5 cm.

DISCUSSION OF RESULTS

The best value for the oscillator strength of the 0-0 band of C_2 obtained by averaging the f values from the emission and absorption data is 0.005 ± 0.003. Self-absorption corrections amount to no more than 4% and are negligible for the emission data on rotational lines. Experimental data and calculated f values are included in Appendix B. King[102] has made an equivalent width measurement of 2.3×10^{-3} Å on $K_P' = 34$ at 5150.6 Å by using a path length of 22 cm and 2840°K. Calculation of the f value by using current thermal data gives an f value of 0.005. King did not correct for emission but corrected for derivations from the linear portion of the curve of growth. He estimates an error in the measurement of approximately 50%. It is estimated by using King's furnace temperature of 2840°K as the reversal temperature and approximating his lamp temperature as 3450°K or 3200°K, that a correction for emission would increase his f value by 25 to 50%.

The best f value is 0.005 ± 0.003, as indicated from this research. This value within the limits of error agrees with the value found from King's data.

ACKNOWLEDGMENTS

The direction of this research by Professor Leo Brewer is gratefully acknowledged. Exposure to his pragmatic philosophy of scientific theory in terms of experimental fact has been a rewarding experience. His weekly seminars have been a particularly useful part of my general graduate training.

I wish to thank Professor Sumner P. Davis, who provided the spectrograph for this research. I am grateful to Professor John G. Phillips for the use of his microphotometer equipment for scanning photographic plates. The advice and guidance provided by both these men is appreciated. Thanks are due Mrs. Pat Cookson and Miss Diane Ota for secretarial assistance. Finally, I acknowledge with especial appreciation the contribution of my husband, Richard Hagan, who gave helpful suggestions for parts of the laboratory work and provided encouragement throughout my graduate studies.

This work was done under the auspices of the U. S. Atomic Energy Commission.

APPENDIX

A. Geometrical Optics Between King Furnace and Concave-Grating Spectrograph

The methods used for imaging the gas emission on the slit are complicated for the King furnace because the graphite tube is an extended source. Thus some of the techniques used in Raman spectra are not applicable because the light cannot pass through the walls of the tube. It is desired to obtain the most effective slit illumination with the exclusion of continuous radiation from the walls. Thus it is usual to focus on the back of the hot zone of the furnace and to use an aperture stop smaller than the tube diameter to eliminate wall light. Since the diaphragm is small, it is necessary to use some kind of lens system to fill the grating horizontally and at the same time cover the slit because the size of the image on the plate is determined by the size of the image on the slit.

A theoretical analysis and some practical application of the problem of focusing cylinders of radiation have been given by Nielsen.[93,94] One of his papers specifically treats the optics for sources of smaller aperture than the slit. To get the maximum amount of radiation from a Raman tube into the spectrograph, Nielsen considered light coming from an inner region determined by planes cutting the slit length, slit width, and collimator aperture. An outer region is determined by the above planes and, in addition, by planes cutting one another in a horizontal line lying at a distance, z_0, in front of the slit. For the coordinate system with reference to the center of the slit as origin,

the z axis coincides with the collimator axis, the x axis is perpendicular, and the y axis is parallel to the slit.

Nielsen derived geometrical functions that are proportional to the amount of light entering the spectrograph. These functions, $F(x,y,z)$, were calculated for the inner and outer regions and for $z_1 < z_0 < z_2$ and thus gave a total of four functions. It was found for the 3-m-grating spectrograph used in the present research that the functions F_1^i, F_2^i, for the inner region for a given z, are independent of the value of x and y. The function, F_1^0, for the outer region increases as x increases and decreases to zero when y = 1.9. The function, F_2^0, also increases as x increases and decreases to zero when y has increased to 2.5. The calculations for the 3-m spectrograph are comparable to those of Nielsen for the Hilger quartz spectrograph. It may be concluded that all source points lying within the inner region and having a given coordinate z are equally effective in sending light into the spectrograph. For a volume element in the outer region, the amount of light sent into the spectrograph decreases almost linearly as the volume element moves from the inner to the outer boundary of this region.

A table of values of x and y for given values of z is included, where $x_0 = \frac{az}{f}$, $y_0 = s - \frac{(b-s)z}{f}$, and $y_1 = s + \frac{(b+s)z}{f}$, and where the length of the slit is 2s, the length of the grating lines is 2a, the width of the grating is 2b, and the focal length of the grating is f.

Table VIII. Values of x_0, y_0, and y_1 for various values of z

z	x_0	y_0	y_1	
40	0.34	0.35	2.14	
59	0.50	0.00	2.63	s = 1.1 cm
60	0.51	0.02	2.66	b = 6.69 cm f = 300. cm
80	0.68	0.39	3.18	a = 2.25 cm
100	0.85	0.76	3.70	

Table IX. Values obtained for the functions F_1^i, F_1^0, for given values of x, y, and z.

F_1^i	x	y	z	F_1^0	x	y	z
0.000984	0.	0.	40	0.001180	0.	0.	40
				0.000961	0.	0.35	40
0.000984	0.85	0.	40	0.001217	0.502	0.	40
0.000984	0.	0.35	40	0.000998	0.502	0.35	40
0.000984	0.502	0.35	40	0.00	0.	1.9	40
0.000632	0.	0.	59				
0.000632	0.502	0.	59				

Table X. Values obtained for the functions F_2^i, F_2^0 for given values of x, y, and z.

F_2^i	x	y	z	F_2^0	x	y	z
0.000344	0.	0.	80	0.000392	0.	0.	80
0.000344	0.502	0.	80	0.000337	0.	0.35	80
0.000344	0.85	0.	80	0.000409	0.502	0.	80
0.000344	0.	0.35	80	0.000354	0.502	0.35	80
0.000344	0.502	0.35	80	0.	0.	2.51	80
				0.	0.502	2.62	80

After integrating the preceding functions with respect to x and y, the functions may be calculated as a function of z, the distance from the slit. By using the equations

$$S_1^i(z) = K\left(1 - \frac{bz}{s(f+z)}\right) , \tag{98}$$

$$S_2^i(z) = K\left(1 - \frac{s(f+z)}{bz}\right) , \tag{99}$$

$$S_1^0(z) = K \frac{bz}{s(f+z)} , \tag{100}$$

$$S_2^0(z) = \frac{Ks(f+z)}{bz} , \tag{101}$$

and

$$K = \frac{2abs}{f^2} , \tag{102}$$

the integrated intensity values normalized to S_1^i equal to unity for z = 0 are obtained, as shown in Table XI.

Table XI. Integrated relative intensities (S_1^i, S_2^i, S_1^0, S_2^0) for various values of z.

z	S_1^i	S_2^i	S_1^0	S_2^0
0	1.	$-\infty$	0.	$+\infty$
5	0.90		0.10	
10	0.80		0.20	
20	0.62		0.38	
40	0.29		0.72	
60		0.013	1.01	0.99
90		0.29		0.71
120		0.42		0.58
160		0.53		0.47
180		0.56		0.44

When $S_1^0 = 0$, $z_0 = 59$ cm. At distances from the slit between 25.9 cm and 147 cm the largest amount of light comes from the outer region, whereas for values smaller than 25.9, or larger than 147, the inner region contributes more light if the source is of uniform brightness and is large enough in cross section to fill both the inner and outer regions. Figure 9 shows these regional variations with respect to z.

The geometry for Nielsen's optics is based on a cylinder of radiation of infinite length. When his results are applied to a finite tube and a system of fixed dimensions, it is found that the focus is not on the back of the tube; therefore his equations do not satisfy the geometrical requirements of the King furnace and 3-m concave-grating spectrograph.

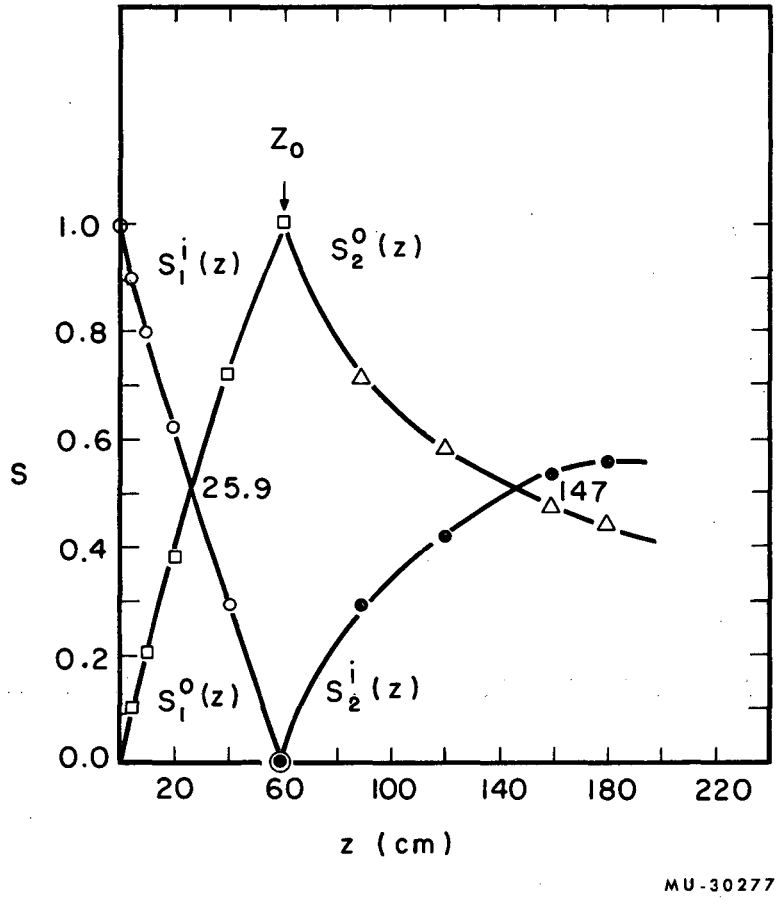

Fig. 9. Functions [S(z)/K] for 3-m grating spectrograph.

For the King-furnace tube only light emitted by the gas is desired, and continuous radiation from the walls should be excluded. Nielsen's calculations, however, do serve as a guide in selecting a low z value which will give a maximum uniform brightness from the tube. It was found from the calculations that the outer-region radiation was not uniform along the slit width and length; thus, radiation from the inner region would be more homogeneous. With the graphite-tube furnace, it is necessary to use lenses fodused on the slit to fill the inner region with light.

Stoicheff and Callomon[95,96] discuss optics for high-resolution Raman spectroscopy. They use two convex lenses placed between the source and the grating as shown in Fig. 10, where h is the tube height, ℓ_t is the length of the tube, ℓ_g is distance from the grating to the slit, f_t and f_g are the focal lengths of the lenses near the tube and near the grating, respectively; s_t is the distance of the image of the back of the tube, s_g is the distance of the image Q to the lens of focal length f_g, and b is the horizontal dimension of the grating. A stop may be placed at the intermediate focus Q. The magnification required for filling the grating is then

$$\frac{f_t}{f_g} = \frac{(NA)_g}{(NA)_t} = \frac{\sin u}{\sin u'} , \tag{103}$$

where u is the half angle of the cones of rays admitted by the spectrograph and u' the half angle for the rays from the tube. The separation of the lenses is given from ordinary lens formulas as

$$s_t = f_t(\ell_z + f_t) \tag{104}$$

and

$$s_g = \frac{f_g(\ell_g + f_g)}{\ell g} . \tag{105}$$

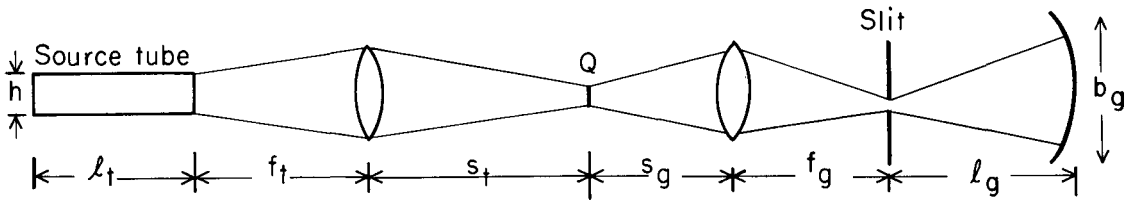

MU-30278

Fig. 10. Optics for high-resolution Raman spectroscopy: h, tube diameter; ℓ_t, tube length; f_t, focal length of lens near tube; S_t, distance of source image to intermediate focus Q; S_g, distance of intermediate focus to lens near grating of focal length f_g; ℓ_g, focal length of concave grating; and b_g, aperture of grating (widest dimension).

For the 3-m-grating spectrograph, the magnification required is 1.62 and from the above equations it is found for a 68-cm distance between tube, lens, and slit that $f_t = 2.92$ cm, $f_g = 1.8$ cm, $s_t = 64.4$ cm, and $s_g = 1.82$ cm, for a given $\ell_t = 60$ cm, $\ell_g = 300$ cm, $(NA)_g = 0.02162$, and $(NA)_t = 0.01334$. It is apparent from this calculation that the image on the slit will be small and that the grating will be flooded with light. The resulting narrow and uneven spectrum[97] is applicable for qualitative analyses but undesirable for quantitative intensity measurements.

To fill the grating with light and at the same time fill the slit, two cylindrical lenses have been used with one spherical lens following a modification of a method used by Hansen and Walsh[98] (see Fig. 11). The cylindrical lens f_1 fills the grating in the horizontal plane; cylindrical lens f_2 fills the grating in the vertical plane. The spherical lens f_3, where f_3 is equal to or greater than the length of the furnace, is used to diverge the light from the tube. It causes the image to be more homogeneous in the vertical plane. Values of the lenses required to fill the numerical aperture of the grating are $f_1 = 6.67$ cm and $f_2 = 16.7$ cm.

To summarize the conditions for the furnace and optics, it is found from Nielsen's equations that the distance from the furnace should be where a maximum of intensity occurs, 59 cm. A larger z minimizes error in quantitative solid-angle calculations of intensity from furnace to slit, as will be shown later. A shorter z gives increased intensity and shorter-exposure times and is more convenient and accurate in alignment of optics. Use of a cylindrical lens in the vertical direction gives a more homogeneous slit illumination and a wider plate image for scanning.

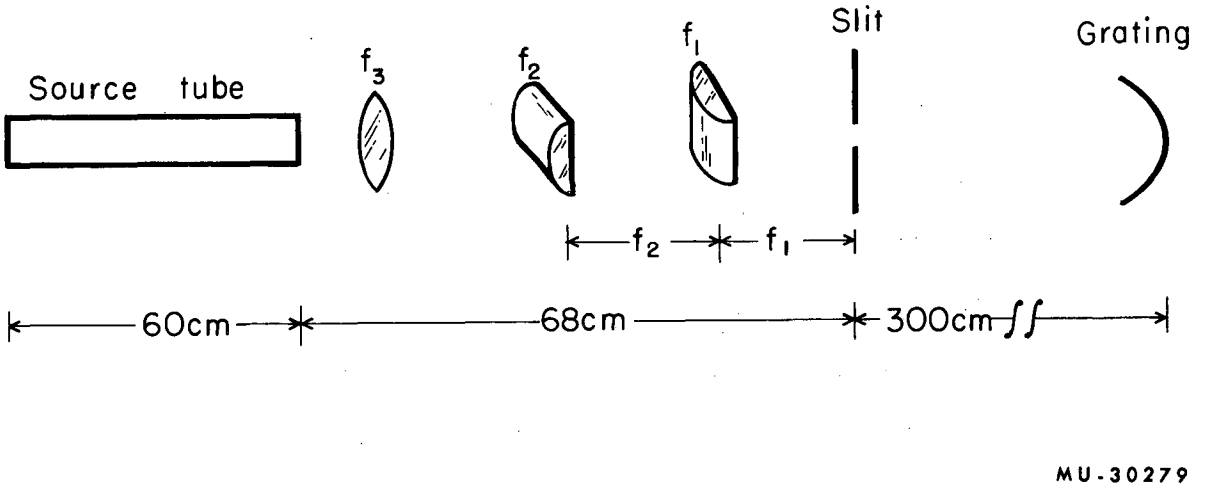

Fig. 11. Schematic diagram for use of cylindrical lenses to satisfy optics requirements of concave grating: f_1, f_2, focal length of cylindrical lenses 1, 2, and f_3, focal length of spherical lens 3.

The measurement of absolute intensity in emission requires consideration of the effect of the geometry of the King-furnace tube on the intensity of light arriving at the slit. It is necessary to compare intensity from the gas in the tube to intensity of a standard source.

For a particular wavelength the spectral emittance of a point-source blackbody per unit frequency interval as given by Eq. (7) in units of quanta per cm^2 per sec per unit solid angle is

$$I = \frac{2}{\lambda^2} \frac{1}{e^{\frac{hc}{\lambda kt}} - 1} . \tag{7}$$

The spectral emittance is the maximum energy originating per cm^2 from a disk within the tube if it acts as a blackbody at this wavelength. This equation may be used for calculating the intensity of the tungsten lamp from the brightness temperature of the lamp. For the intensity of emission from the gas molecules within the tube in units of quanta per cm^2 per sec per unit solid angle, Eq. (18) is used:

$$I^{u\ell} = N' \ell \frac{A}{4\pi} . \tag{18}$$

The density of gas and therefore the intensity are constant for a given temperature and pressure in the furnace tube. The geometrical relations of interest are those required of the intensity on the plate to the intensity of the gas within the furnace and to the intensity from the lamp or blackbody plug. The radiation finally arriving at the plate will be less than the radiation in the tube. The volume of gas in the tube is known. The volume of gas which emits light visible to the slit must be calculated. If the energy of the standard source (blackbody or tungsten lamp) passed through the same optics and were of the same

extension as the gas emitting along the tube, the factors relating the spectral emittance to the irradiance would be equal for the blackbody and for the gas. However, the solid angle of light for the gas is not identical to that for the blackbody because the gas is an extended source. However, the geometry of the gas and the standard source may be calculated by making assumptions about the extent and position of the standard source.

The radiant flux of intensity per unit volume for a gaseous source is $I^{u\ell}$. The intensity relation for an extended source is required when a surface receives radiant energy from more than one source. The total radiant energy falling on the surface is the arithmetic sum of the energies produced by the sources. The irradiance H from a point source on an area ΔA is

$$H = \frac{I\cos\Theta}{r^2}, \tag{106}$$

where Θ is the angle made by the normal of an element of surface dA with the distance r to a point source S. The irradiance from a circular disk of diameter of the King-furnace tube on an element of area dA a distance ℓ from an extended source may be calculated.

Substitutions in Eq. (106) are made for r in terms of the distance on the normal b between the disk and the irradiated area and $r^2 = a^2 + b^2$, where a is the radius of the disk. The intensity if equal to the emittance per unit area times the area of the disk. The angle Θ is assumed equal to zero. The irradiance for the disk is then

$$H = \frac{I^{u\ell}(\pi a^2)}{(a^2 + b^2)} . \tag{107}$$

At distances sufficiently large for a^2 to be negligible compared with b^2, the equation reduces to the inverse-square law, as for a point source. For example, if a is one-tenth of b , then a^2 is only one percent of b^2, and an error of one percent is introduced if a^2 is neglected in the denominator. Thus, a circular disk can be considered a point source at any distance greater than ten times its radius within an accuracy of 1%.

For one-size King-furnace tube a = 0.8, b = 93 to 103 cm, $\frac{a}{b}$ = 0.86%. Therefore, for the King furnace the diameter of the disk may be treated as a point source for the slit, so long as the furnace disk in question is more than 8cm away from the slit. Since only the inner part of the tube emits light, this condition will always be fulfilled, and the irradiance is

$$H = \frac{I^{u\ell}\pi a^2}{b^2} . \qquad (108)$$

The variation in intensity for a disk from the center and from the edge may be calculated from tables, by Masket et al, of solid angles subtended by a circular disk.[99] For the 0.8-cm-radius tube with the geometry (see Fig. 12) of the King furnace and a point 106 cm from the slit, the geometrical factors are found for axial illumination, 0.136309×10^{-2} and for off-axis (0.8 cm) illumination, 0.136295×10^{-2}. The radius of the tube and the distance z are normalized then by the radius of the image on the slit, 2.23 cm. The off-axis illumination is found to be 0.01% of the axial illumination; therefore the disk may be treated as a point source.

The contribution of the axial length of the tube must be calculated.

Since the above equation was for a circular disk, it must be integrated with respect to z. This must be done from the geometry of Fig. 12, where L_1 is the distance of the front of the furnace to the slit, L_2 is the distance of the furnace window to the front of the emitting zone, and z is the length along the hot zone. The irradiance for the entire zone is then

$$H_{total} = \int_0^L \frac{I^{u\ell}\pi a^2}{(z + L_1 + L_2)^2}\, dz, \tag{109}$$

where $(z + L_1 + L_2)$ is the distance of the emitting disk from the slit and is now a variable, and L is the length of the hot zone. To integrate, it is convenient to change variables; let

$$z' = z + L_1 + L_2 , \tag{110}$$

$$H_{total} = I^{u\ell}\pi a^2 \int_{L_1+L_2}^{L_1+L_2+L} \frac{1}{(z')^2}\, dz' \tag{111}$$

$$= I^{u\ell}\pi a^2 \frac{L}{(L_1+L_2)(L_1+L_2+L)} . \tag{112}$$

The contribution due to finite z is computed by taking a ratio of $\frac{H_{total}}{H_{disk}}$, where $b = L_1 + L_2$. For $L_1 = 68$ cm, $L_2 = 23$ cm, $L = 15$ cm, it follows that

$$\frac{H_{total}}{H_{disk}} = \frac{L(L_1+ L_2)}{(L_1+L_2+L)} = \frac{15(91)}{106} = 1.288. \tag{113}$$

Therefore the error introduced if the finite extent of the tube were ignored is approximately 29%.

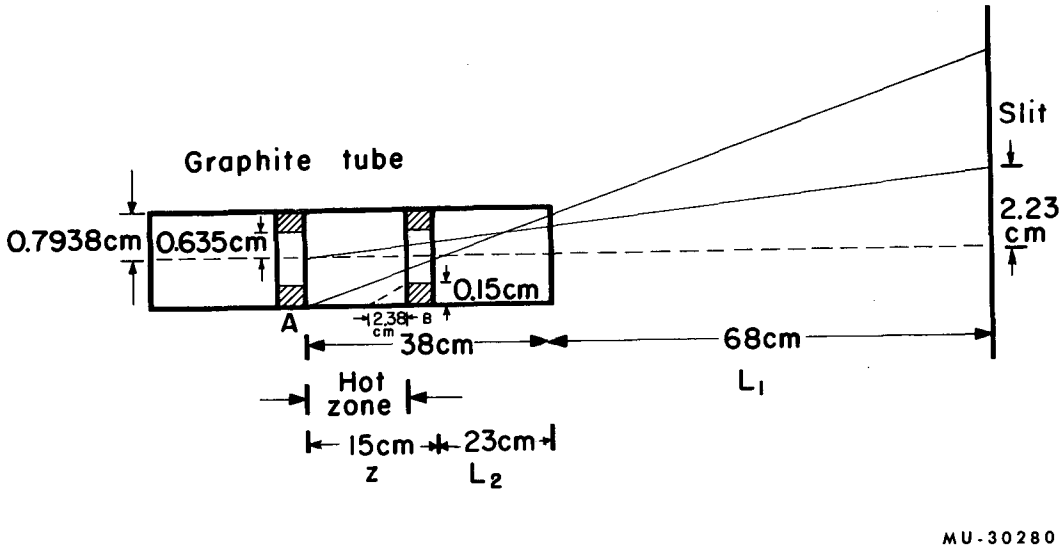

Fig. 12. Geometrical optics of King furnace. Vertical dimension greatly enlarged to show divergence of beam: A, back baffle; B, front baffle; z, heating zone; L_1, distance from furnance window to slit; and L_2, distance from front baffle to furnance window.

As a first approximation the geometry effect upon the irradiance arriving at the slit from the furnace tube in the absence of stops and lenses will be calculated. The situation in the King furnace is complicated by the presence of baffles which cause the volume to be slightly different from that of a cylinder, or from that in Fig. 12. If the end of a 0.7938-cm-radius tube is used as the only stop, then some of the light in the tube does not arrive at the slit because of the baffle. It is necessary to calculate this limiting angle and the distance from the baffle inside the tube from which no light arrives at the slit. From this geometry it is seen that the distance from the baffle to the inside of the tube where the light begins to emerge is 2.38 cm. Then for the large cylinder of radius 0.7938 cm, the irradiance is calculated for a tube distance of 12.62 cm. For this region all of the light in the tube gets to the slit:

$$H = 2.5238 \times 10^{-3} I^{u\ell}. \tag{114}$$

Then in the front of the tube the total available irradiance is calculated:

$$H = 0.4884 \times 10^{-3} I^{u\ell}. \tag{115}$$

From a cylinder having the radius of the baffle all of the light arrives at the slit; the irradiance is

$$H = 0.3125 \times 10^{-3} I^{u\ell}. \tag{116}$$

Subtracting the inner from the outer cylinder gives the effect of the torus of length 2.38 cm and outside diameter 0.7938 cm, inner diameter 0.635 cm. This gives $0.1759 \times 10^{-3} I^{u\ell}$, which is divided by two since only one-half of the torus contributes to the irradiance at the slit.

Addition of the separate contributions gives the total irradiance per cm^2 at the slit to be $2.9343 \times 10^{-3} I^{u\ell}$.

For a plug at the center of the furnace for the 0.8-cm-radius tube, with L equal to 7 cm rather than 15 cm, the irradiance may be calculated by considering the source as extended. The result is $1.39980 \times 10^{-3} I^{u\ell}$.

If the plug is considered as a disk without extent along the z axis, the equation reduces to

$$H = \frac{I^{u\ell} \pi a^2}{b^2}, \tag{108}$$

which gives $0.2061 \times 10^{-3} I^{u\ell}$. If the back of the hot zone rather than the center of the tube is used, the irradiance is $0.1761 \times 10^{-3} I^{u\ell}$.

For the lamp it may be assumed that the volume from the tube limited by the baffles contributes to the intensity at the slit. For the calculation the total tube length L is used; this gives an upper limit to the irradiance at the slit, $8.7318 \times 10^{-3} I^{u\ell}$. If the irradiance from the lamp is calculated for a disk at the front of the furnace, the result is $0.2739 \times 10^{-3} I^{u\ell}$. As a lower limit the disk may be considered to be at the back of the furnace; the calculation then gives the result, $0.0773 \times 10^{-3} I^{u\ell}$. The results are summarized in Table XII.

To get the irradiance relation from the slit to the plate, the intensity per unit area of the grating may be calculated because the intensity per unit area on the slit is known. The effect of lenses will be to expand the image and therefore decrease the intensity per unit area. This effect may be calculated from the particular lens system used.

Table XII. Geometry contributions to irradiance at slit from furnace.

Geometry	Irradiance
Volume effect of tube for gas in hot zone	$2.9243 \times 10^{-3}\ I^{u\ell}$
Volume effect for plug in center of hot zone	$1.3998 \times 10^{-3}\ I^{u\ell}$
Area effect for plug as disk at center of tube	$0.2061 \times 10^{-3}\ I^{u\ell}$
Area effect for plug as disk at back of hot zone	$0.1762 \times 10^{-3}\ I^{u\ell}$
Volume effect of tube for lamp at back of furnace	$8.7318 \times 10^{-3}\ I^{u\ell}$
Area effect for lamp as disk at front of furnace	$0.2739 \times 10^{-3}\ I^{u\ell}$
Area effect for lamp as disk at back of furnace	$0.0773 \times 10^{-3}\ I^{u\ell}$

The length of the slit required for maximum intensity for a concave grating may be found.[100, 101] The slit length is

$$\ell' = \ell \left(\frac{\sin^2 \beta \cos \alpha}{\cos \beta} + \sin^2 \alpha \right) , \qquad (117)$$

where the angle of incidence α is equal to the angle of diffraction β, and ℓ is the length of the grating lines. For $\alpha = \beta = 30^\circ$ and $\ell = 5$ cm, $\ell' = 2.5$ cm. The actual slit length is 2.2 cm. As a result of the astigmatism, a point on the slit is imaged as a line whose length z is obtained by multiplying the length ℓ of the ruled lines on the grating by a factor k such that

$$z = (\sin^2 \beta + \sin \alpha \tan \alpha \cos \beta)\ell = k\ell . \qquad (118)$$

For the Eagle mounting, when $\alpha = \beta = 30^\circ$, then $z = \ell/2$, $k = 1/2$, and

and therefore z = 2.5 cm, which is the optimum slit length. It may be concluded, therefore, that for a slit length equal to the length of the line on the plate, by assuming uniform slit illumination from a blackbody source that just fills the grating, the intensity per unit area on the slit will be proportional to the intensity per unit area of the line on the plate.

For the concave grating the condition for reinforcement of rays is

$$n\lambda = d(\sin \alpha + \sin \beta) \tag{119}$$

where n is the order of the spectrum and d is the distance between grating lines. Since $\alpha = \beta$ for the Eagle mounting, these angles can be calculated for a given wavelength. For 5000Å there is found an angle of incidence and reflection of $8^{\circ}29'$ and in second order an angle of $17^{\circ}6'$. For an angle of 15°, the slit length for maximum intensity is 6.699 cm. This length is much longer than the actual slit length; however, the theoretical slit length gives maximum intensity, but the area of illumination on the slit defines the area of homogeneous plate blackening. The image appears somewhat larger because of the spherical astigmatism of the grating mirror. It is assumed that the grating optics will not affect the spectra in a manner different from the standard source when light is focused on the grating from an outer limiting stop. This outer limiting aperture is the same, of course, for the gas and the standard source.

The experimental results are subject to other errors previously discussed which seem to obscure the influence of geometrical optics. Experiments indicated that the use as a reference source of the

tungsten lamp or of the blackbody plug gave comparable results. It is concluded, therefore, that the difference in geometry between the reference source and the gas did not affect the results within the limits of error of the experimental data.

APPENDIX

B. Tables of Experimental Data

The experimental ratios a measured from the plates and scans, are given in Tables XIII through XVIII. Measurements are given by plate number and exposure number on the plate; scans to the violet and to the red through the feature are listed separately. The ratios a are the experimentally measured ratios $\frac{I_{em}^{net}}{I_{BB}}$, $\frac{I_{abs}^{net}}{I_{lamp}}$, or $\frac{I_{em}^{net}}{I_{lamp}}$. The ratio α defined by Eq. (82), corrects absorption data for emission; k is the final absorption ratio, which includes concentration corrections for measured ratios off the linear region of the curve of growth. For emission data and for absorption data, Eqs. (79) and (90), respectively, were used to calculate f values. For all emission data the ratio a was used in the calculations; for emission ratios of rotational lines a^R refers to lines K' = 16 or 18 in the R branch, and a^P to lines K' = 43 or 45 in the P branch. The ratio Q is defined by Eqs. (56) and (64). For the absorption data some of the ratios were remeasured at a later time. The remeasured values are in parenthesis; emission measurements are starred.

Values in Table XVIII are considered inaccurate because of the uncertainty in the reversal temperature, and because the magnitude of absorption was of the order of the background fluctuation due to grain size of the 103a-F photographic plates. Agreement is observed for emission results obtained from 103a-F and IIa-F photographic plates and photomultiplier scans, and for absorption results on the smaller-grained IIa-F plates.

Self-absorption corrections for the head were obtained in a manner similar to the one described for individual rotational lines described in the section on analysis of data. Equation (64) was used to obtain the corrections for self-absorption,

$$Q = 1 + \frac{1}{2\sqrt{2}} R_0, \tag{64}$$

and R_0 was determined as described below. From a plot of $\frac{I_J}{I_{band}}$ as a function of wave number for each rotational line near the C_2 head, and by assuming a Doppler width of 0.15 cm^{-1}, a Doppler profile was found for the band near the head. At the head the Doppler profile, obtained from the graphical summation of overlapping rotational lines, has a fairly constant intensity within a 0.15-cm^{-1} range and decreases significantly on either side. A similar plot was made for lines instrumentally broadened to a half-width of 1.0 cm^{-1}. The true peak intensity is 3.39 times as high as the instrumental peak intensity. Peak heights for the instrumentally-broadened heads are measured experimentally. The ratio R_0 is defined as

$$R_0 = \frac{I_{0Dop}}{I_{BB}} = \left(\frac{I_{instr}}{I_{BB}}\right) 3.39, \tag{120}$$

where $\frac{I_{0Dop}}{I_{BB}}$ was used for the individual rotational lines and $\frac{I_{instr}}{I_{BB}} \cdot (3.39)$ for the head. The ratio $\frac{I_{instr}}{I_{lamp}}$ was measured experimentally and is multiplied by $\frac{I_{lamp}}{I_{BB}}$, where I_{BB} is the intensity of a lamp at reversal temperature:

$$R_0 = \left(\frac{I_{instr}}{I_{lamp}}\right)\left(\frac{I_{lamp}}{I_{BB}}\right) 3.39 \quad . \tag{121}$$

The value for Q, the ratio of the true peak to the measured peak is now obtainable. The self-absorption at the head is shown in Tables XVII and XVIII.

Table XIII. Emission data for rotational lines $K'_P = 43$, $K'_R = 16$ of C_2 0-0 Swan band.*

Plate	T (°K)	a^R	Q	f	a^P	Q	f
55n	2848 (low)	0.1045	1.04	0.0184	0.0661	1.02	0.0183
	3026 (high)	0.0981	1.03	0.0025	0.0725	1.03	0.0025
83n	2979 (lamp)	0.0873	1.03	0.0032	0.0608	1.02	0.0032
	2993 (furnace)			0.0033			0.0033
90n	3018	0.0824	1.03	0.0023	0.0609	1.02	0.0023
101n	2888	0.0427	1.02	0.0045	0.0285	1.01	0.0046
103n	2893	0.0509	1.02	0.0053	0.0335	1.01	0.0052
100n	2888	0.0418	1.01	0.0044	0.0271	1.01	0.0043
102n	2888	0.0606	1.02	0.0064	0.0392	1.01	0.0063

* The average f value for both Tables XIII and XIV is 0.006 ± 0.004.

Table XIV. Emission data for rotational lines $K'_P = 45$, $K'_R = 18$ of C_2 0-0 Swan band.*

Plate	T (°K)	a^R	Q	f	a^P	Q	f
55n	2848 (low)	0.1237	1.04	0.0206	0.0640	1.02	0.0199
	3026 (high)	0.1173	1.04	0.0028	0.0704	1.02	0.0027
83n	2979 (lamp)	0.0903	1.03	0.0032	0.0530	1.02	0.0031
	2993 (furnace)						0.0032
90n	3018	0.0914	1.03	0.0024	0.0573	1.02	0.0024
101n	2888	0.0452	1.02	0.0045	0.0248	1.01	0.0044
103n	2893	0.0559	1.03	0.0055	0.0310	1.01	0.0054
100n	2888	0.0376	1.01	0.0037	0.0209	1.01	0.0037
102n	2888	0.0749	1.03	0.0076	0.0392	1.01	0.0070

* The average f value for both Tables XIII and XIV is 0.006 ± 0.004.

Table XV. Emission data for rotational lines $K'_P = 43$, $K'_R = 16$ of C_2 0-0 Swan band *

Scans	T (°K)	a^R	Q	f	a^P	Q	f
to violet	2963	0.0595	1.02	0.0028	0.0446	1.02	0.0029
	2988			0.0024			0.0025
to red	2963	0.0833	1.03	0.0039	0.0595	1.02	0.0039
	2988			0.0034			0.0033

* The average f value for both Tables XV and XVI is 0.004 ± 0.0007.

Table XVI. Emission data for rotational lines $K'_P = 45$, $K'_R = 18$ of C_2 0-0 Swan band.*

Scans	T (°K)	a^R	Q	f	a^P	Q	f
to violet	2963	0.0952	1.03	0.0045	0.0565	1.02	0.0037
	2988			0.0039			0.0031
to red	2963	0.1161	1.04	0.0055	0.0714	1.03	0.0048
	2988			0.0048			0.0040

* The average f value for both Tables XV and XVI is 0.004 ± 0.0007.

Table XVII. Absorption and emission data for the C_2 0-0 Swan-band head.

II-aF Plate	Exp. No.	T_{rev} 5165Å (°K)	T_{lamp} 5165Å (°K)	a	α	k	Q	f^{abs}	f^{em}	f^{em}(s.a.)
77b	2	3046±25	3186	0.024	0.073	0.076		0.0062		
	3	"	3186	0.020	0.061	0.062		0.0051		
*	5	"	2893	0.13			0.10		0.0068	0.0075
*78b	1	"	2899	0.10			1.08		0.0054	0.0058
*	2	"	2984	0.27			1.27		0.0190	0.0242
*79b	1	"	2920	0.09			1.07		0.0052	0.0088
				(0.07)			1.07		0.0052	0.0088
*	2	"	3020	0.03			1.03		0.0024	0.0031
				(0.03±0.005)			1.03		0.0024	0.0031
	3	"	3134	0.013 (very small)	0.057	0.059		0.0048		
	4	"	3208	0.014	0.031	0.031		0.0025		
	5	"	3208	0.012	0.026	0.026		0.0021		
				(0.006±0.003)	0.013	0.013		0.0011		
*80b	1	"	2884	0.13			1.09		0.0066	0.0072
				(0.13±0.03)			1.09		0.0066	0.0072
*	2	"	2884	0.035			1.03		0.0018	0.0023
				(0.034)			1.03		0.0018	0.0023

Table XVII. Absorption and emission data for the C_2 0-0 Swan-band head. (continued)

II-aF Plate	Exp. No.	T_{rev} 5165Å (°K)	T_{lamp} 5165Å (°K)	a	α	k	Q	f^{abs}	f^{em}	f^{em}(s.a.)
80b	3	3046±25	3223	0.006 (very small)	0.015	0.015		0.0012		
	4	"	3223	0.04	0.102	0.108		0.0089		
				(0.065±0.005)	0.165	0.180		0.0151		
	5	"	3223	0.05	0.127	0.136		0.0111		
				(0.007±0.005)	0.018	0.018		0.0015		
						Average f values		0.005±0.003	0.006±0.003	0.005±0.002

*emission

rescan values (in parentheses)

s.a. (self-absorption)

Table XVIII. Absorption and emission data for the C_2 0-0 Swan-band head.

103a-F Plate	Exp. No.	T_{rev} 5165Å (°K)	T_{lamp} 5165Å (°K)	a	α	k	Q	f^{abs}	f^{em}	f^{em}(s.a.)
48b	2	2889±130	3210	0.0363 (very small)	0.059	0.061		0.028		
	3	2889	3123	0.0393	0.077	0.080		0.036		
				(0.0129)	0.025	0.025		0.011		
*51b	1	2889	2756	0.1218			1.09		0.036	0.040
	3	3027	3202	0.1566	0.400	0.509		0.052		
52b	1	3081	3232	0.1045	0.304	0.362		0.023		
*	2	3107	3004	0.2192			1.19		0.086	0.100
				(0.1822)			1.16		0.072	0.084
	3	3134	3208	0.0725	0.247	0.284		0.011		
				(0.066±0.03)	0.225	0.255		0.011		
53b	2	3027	3199	0.15±0.04	0.388	0.489		0.050		
*	3	3027	2783	0.34			1.33		0.016	0.021
54b	1	3027	3199	0.18±0.1	0.465	0.622		0.063		
	2	3027	3204	0.20±0.09	0.510	0.708		0.072		
	3	3027	3205	0.08±0.03	0.199	0.222		0.222		
*56b	2	3107	2952	0.68±0.05			1.50		0.023	0.034
31b		3121	3449	0.17±0.1	0.300	0.357		0.015		
32b		3121	3449	0.18±0.1	0.312	0.374		0.016		
64b	2	2995±20	3189	0.0786	0.183	0.203		0.030		

Table XVIII. Absorption and emission data for the C_2 0-0 Swan-band head. (continued)

103a-F Plate	Exp. No.	T_{rev_o} 5165Å (°K)	T_{lamp} 5165Å (°K)	a	α	k	Q	f^{abs}	f^{em}	f^{em}(s.a.)
64b	2	2995±20	3189	(0.03±0.01)	0.070	0.073		0.011		
							Average f value	0.030±0.02	0.047±0.026	0.056±0.029

* emission

rescan values (in parentheses)

s.a. (self-absorption)

REFERENCES

1. D. F. Swinehart, J. Chem. Ed. 39, 333 (1962).
2. W. Kauzmann, Quantum Chemistry (Academic Press, Inc., New York, 1957), p. 646.
3. A. C. Mitchell and M. W. Zemansky, Resonance Radiation and Excited Atoms (Cambridge University Press, New York, 1961), pp. 96, 170.
4. G. Herzberg, Spectra of Diatomic Molecules (D. Van Nostrand Company, Inc., Princeton, N. J., 1959).
5. R. S. Mulliken and C. A. Rieke, Rept. Progr. Phys. 8, 231 (1941), p. 232.
6. See reference 2, p. 655.
7. See reference 2, p. 651.
8. H. A. Bethe and E. E. Saltpeter, Handbuch der Physik Atoms I, 35, 88 (1957), p. 342.
9. W. Thomas, Naturwiss 13, 627 (1925).
10. F. Reiche, see reference 9.
11. W. Kuhn, Z. Physik 33, 408 (1925).
12. V. N. Soshnikov, Soviet Phys. Usp. 4, No. 3, 425 (1961), p. 426.
13. D. Robinson and R. W. Nicholls, Intensity Measurements on Overlapped Molecular Bands, Air Force Cambridge Research Center, AFCRC-TN 58-456, (1958).
14. A. Einstein, Physik Z. 18, 121 (1917).
15. See reference 5, p. 200.
16. E. U. Condon and G. H. Shortley, The Theory of Atomic Spectra (University Press, Cambridge, 1959), p. 238.
17. See reference 5, pp. 208, 73.

18. R. Ladenburg and F. Reiche, Ann. Physik 42, 181 (1913).

19. R. B. King and A. S. King, Astrophys. J. 82, 427 (1935).

20. R. B. King and A. S. King, Astrophys. J. 87, 359 (1938).

21. A. Unsöld, Physik der Sternatmosphären (Verlag von Julius Springer, Berlin, 1938), J. W. Edwards, Publishers, Inc., Ann Harbor, Michigan.

22. R. B. King and D. C. Stockbarger, Astrophys. J. 91, 193 (1940).

23. W. T. Hicks, Spectroscopy of High Temperature Systems (Ph.D. Thesis), University of California Lawrence Radiation Laboratory Report UCRL-3639, Feb. 1957.

24. See reference 3, p. 99.

25. R. C. Johnson and N. R. Tawde, Proc. Roy. Soc. 137A, 575 (1932).

26. A. G. Gaydon and H. G. Wolfhard, Proc. Roy. Soc. 201A, 570 (1950).

27. A. G. Gaydon and H. G. Wolfhard, Proc. Roy. Soc. 194A, 169 (1948).

28. B. B. Laud, Ph.D. Thesis, Bombay University, 1951.

29. J. M. Patel, Ph.D. Thesis, Bombay University, 1947.

30. N. R. Tawde and J. M. Patel, Bombay Univ. J. VI, Part II, 29 (1937).

31. N. R. Tawde and B. B. Laud, Proc. Natl. Inst. Sci. India 20A, 259 (1954).

32. R. B. King, Astrophys. J. 108, 429 (1948).

33. J. G. Phillips, Mem. Soc. Roy. Sci. Liege 14 III, 452 (1954).

34. J. G. Phillips, Astrophys. J. 125, 153 (1957).

35. R. H. Lyddane, F. T. Rogers, and F. E. Roach, Phys. Rev. 60, 281 (1941).

36. J. U. White, J. Chem. Phys. 8, 79 (1940).

37. G. Stephenson, Proc. Phys. Soc. (London) 64A, 99 (1951).

38. R. S. Mulliken, Rev. Mod. Phys. 4, 1 (1932).

39. C. A. Coulson, Valence (Oxford University Press, N. Y., 1960), p. 90, 100.

40. H. Shull, J. Chem. Phys. 20, 1095 (1952).

41. H. Shull, Astrophys. J. 114, 546 (1951).

42. H. Shull, Astrophys. J. 112, 352 (1950).

43. C. A. Coulson and G. R. Lester, Trans. Faraday Soc. 51, 1605 (1955).

44. E. Clementi, Astrophys. J. 132, 898 (1960).

45. R. S. Mulliken, J. Phys. Chem. 56, 295 (1953).

46. M. E. Pillow, Mem. Soc. Roy. Sci. Liege 13, 145 (1953).

47. M. E. Pillow, Proc. Phys. Soc. (London) 64A, 772 (1951).

48. P. M. Morse, Phys. Rev. 34, 57 (1929).

49. A. G. Gaydon and R. W. Pearse, Proc. Roy. Soc. (London) 173A, 37 (1939).

50. Ta-You Wu, Proc. Phys. Soc. 65A, 965 (1952).

51. G. Wentzel, Z. Physik, 38, 518 (1926).

52. H. A. Kramers, Z. Physik 39, 828 (1926).

53. L. Brillouin, J. Phys. Radium 7, 353 (1926).

54. A. A. Wyller, Mem. Soc. Roy. Sci. Liege 13, 137 (1953).

55. H. M. Hulburt and J. O. Hirschfelder, J. Chem. Phys. 9, 61 (1941).

56. H. M. Hulburt and J. O. Hirschfelder, J. Chem. Phys. 35, 1901 (1961).

57. E. Hutchisson, Phys. Rev. 37, 45 (1931).

58. K. Wurm, Z. Astrophys. 5, 260 (1932).

59. A. McKellar and W. Buscombe, Publ. Dominion Astrophys. Obs. Victoria 7, 361 (1949).

60. N. Tawde and J. Patel, Astrophys. J. 112, 210 (1950).

61. A. McKellar and N. R. Tawde, Astrophys. J. 113, 440 (1951).

62. N. Tawde and V. Rajeswari, J. Sci. Ind. Res. (India) 14B, 302 (1955).

63. D. R. Bates, Monthly Notices Roy. Astron. Soc. 112, 614 (1952).

64. P. Fraser, W. Jarmain, and R. Nicholls, Astrophys. J. 119, 286 (1954).

65. R. W. Nicholls, Proc. Phys. Soc. (London) 69A, 741 (1956).

66. R. W. Nicholls, Ann. Geophys. 14, 208 (1958).

67. W. R. Jarmain, Can. J. Phys. 38, 217 (1960).

68. W. R. Jarmain, Tabulated Klein-Dunham Potential-Energy Functions for Fifteen States of N_2, N_2^+, NO, O_2, C_2, and OH, Geophysical Research Directorate and Air Force Office of Scientific Research, GRD-TN-60-498, AFOSR-TN-60-877 (1960).

69. W. R. Jarmain, Tabulated Klein-Dunham Potential-Energy Functions for Teh States of C_2 (4), O_2 (2), OH (2), and SiO (2), Air Force Cambridge Research Center and Air Force Office of Scientific Research, AFCRL-682, AFOSR-1124 (1961).

70. N. L. Singh and D. C. Jain, Can. J. Phys. 40, 520 (1962).

71. S. M. Read and J. T. Vanderslice, J. Chem. Phys. 36, 2366 (1962).

72. See reference 39, pp. 140 through 151.

73. L. Brewer, P. W. Gilles, and F. A. Jenkins, J. Chem. Phys. 16, 797 (1948).

74. J. L. Engelke, High Temperature Studies of the C_3 Molecule (Ph.D. Thesis), University of California Lawrence Radiation Laboratory Report UCRL-8727, April 1959.

75. O. H. Krikorian, High Temperature Studies III. Heat of Formation of the $^3\Pi_u$ State of C_2 from Graphite (Ph.D. Thesis), University of California Lawrence Radiation Laboratory Report UCRL-2888, April 1955.

76. R. A. Sawyer, Experimental Spectroscopy (Prentice-Hall, New York, 1946), p. 128.

77. D. R. Lovejoy, Can. J. Phys. 36, 1397 (1958).

78. H. Moser, G. Otto, and W. Thomas, Z. Physik 147, 76 (1957).

79. J. W. DuMond and E. R. Cohen, Rev. Mod. Phys. 25, 691 (1953).

80. C. R. Barber, J. Sci. Instr. 23, 238 (1946).

81. D. R. Lovejoy, International Congress Pure and Applied Chemistry (1961), p. 149.

82. E. F. Worden, Jr., High Intensity Light Sources (Ph.D. Thesis), University of California Lawrence Radiation Laboratory Report UCRL-8509, Oct. 1958.

83. H. G. Beutler, J. Opt. Soc. Am. 35, 311 (1945), pp. 327, 329.

84. J. G. Phillips, Astrophys. J. 119, 274 (1954).

85. Cary Model-31 Vibrating-Reed Electrometer Instruction Manual, Applied Physics Corportion, Monrovia, California.

86. F. A. Jenkins and H. E. White, Fundamentals of Optics (McGraw-Hill Book Co., Inc., New York, 1957), p. 250.

87. J. C. De Vos, Physica 20, 690 (1954); Fig. 6.

88. R. C. Johnson, Phil. Trans. Roy. Soc. (London) 226A, 157 (1927).

89. A. Budo, Z. Physik 98, 437 (1936).

90. J. G. Phillips, Astrophys. J. 108, 434 (1948), p. 448.

91. K. S. Pitzer and E. Clementi, J. Am. Chem. Soc. 81, 4477 (1959).

92. L. Brewer, W. T. Hicks, and O. H. Krikorian, J. Chem. Phys. 36, 182 (1962).

93. J. R. Nielsen, J. Opt. Soc. Am. 20, 701 (1930).

94. J. R. Nielsen, J. Opt. Soc. Am. 37, 494 (1947).

95. B. P. Stoicheff, Advances in Spectroscopy 1, 168 (1959); Can. J. Phys. 32, 330 (1954).

96. J. H. Callomon, Can. J. Phys. 34, 1046 (1956).

97. R. W. B. Pearse and A. G. Gaydon, The Identification of Molecular Spectra (Chapman and Hall, Ltd., London, 1950), p. 259.

98. G. Hansen, Optik 6, 337 (1950); J. W. Walsh, Optik 15, 457 (1958); and G. R. Harrison, R. C. Lord, and J. R. Loofbourow, Practical Spectroscopy (Prentice-Hall, Inc., Englewood Cliffs, N. J., 1959), p. 129.

99. A. V. H. Masket, R. L. Macklin, and H. W. Schmitt, Tables of Solid Angles and Activations, Oak Ridge National Laboratory Report ORNL-2170, (1956); A. V. H. Masket, Rev. Sci. Instr. 28, 191 (1957).

100. H. G. Beutler, J. Opt. Soc. Am. 35, 311 (1945), p. 331.

101. R. A. Sawyer, Experimental Spectroscopy (Prentice-Hall, Inc., New York, 1946), p. 130.

102. R. B. King, Private Communication.

This report was prepared as an account of Government sponsored work. Neither the United States, nor the Commission, nor any person acting on behalf of the Commission:

A. Makes any warranty or representation, expressed or implied, with respect to the accuracy, completeness, or usefulness of the information contained in this report, or that the use of any information, apparatus, method, or process disclosed in this report may not infringe privately owned rights; or

B. Assumes any liabilities with respect to the use of, or for damages resulting from the use of any information, apparatus, method, or process disclosed in this report.

As used in the above, "person acting on behalf of the Commission" includes any employee or contractor of the Commission, or employee of such contractor, to the extent that such employee or contractor of the Commission, or employee of such contractor prepares, disseminates, or provides access to, any information pursuant to his employment or contract with the Commission, or his employment with such contractor.